Glycerolipids track sinking particle sources and remineralization in two ocean basins

Henry C. Holm[a,b*], Helen F. Fredricks[a], and Benjamin A. S. Van Mooy[a]

Affiliations:

[a]Marine Chemistry and Geochemistry Department, Woods Hole Oceanographic Institution; Woods Hole, MA 02543, USA

[b]MIT-WHOI Joint Program in Oceanography/Applied Ocean Science & Engineering; Cambridge, MA, 02139, USA

*Corresponding author. Email: hholm@ldeo.columbia.edu

Article Title: Glycerolipids track sinking particle sources and remineralization in two ocean basins

Author names: Henry C. Holm[a,b*1], Helen F. Fredricks[a], and Benjamin A. S. Van Mooy[a]

Affiliations:

[a] Marine Chemistry and Geochemistry Department, Woods Hole Oceanographic Institution; Woods Hole, MA 02543, USA

[b] MIT-WHOI Joint Program in Oceanography/Applied Ocean Science & Engineering; Cambridge, MA, 02139, USA

*Corresponding author. Email: hholm@ldeo.columbia.edu Cell: 1(617)-281-6498

[1] Present Address: Lamont-Doherty Earth Observatory, Columbia University, Palisades, NY 10964, USA.

Abstract: The biological carbon pump is a major control on ocean carbon storage. On long time scales, changes in the biological carbon pump modulate atmospheric CO_2 concentrations and climate. Attenuation in sinking carbon fluxes is derived from a combination of remineralization by bacteria, zooplankton, and fragmentation. However, the importance of these attenuation processes varies spatially and temporally. Constraining future changes to the biological carbon pump will therefore require improved knowledge of sinking particle dynamics. In this study we used high resolution mass spectrometry to measure glycerolipid compositions of sinking material from both the Pacific and Atlantic Oceans. These compositions revealed both sources and remineralization processes influencing the lipid fluxes. Most of the lipid carbon from sinking particles appears to be lost non-selectively; these results differ from previous reports of selective degradation in sinking lipids. In both ocean basins, we find that triacylglycerols are transferred better to depth than other glycerolipids. Utilizing a lipid class found almost entirely in phytoplankton, we show that there is a selection for saturated lipids at the onset of particle formation. Lastly, we use the compositions of isolated single particles to train a linear discriminant function that predicts the relative amounts of sinking material derived from fecal pellets versus

aggregates. This new source metric implies that zooplankton reworking is a major control on lipid degradation. We discuss these results in the context of other flux observations and their future applications to study of the biological carbon pump.

Keywords: lipidomics, biological carbon pump, phytoplankton, marine snow, intact polar lipids

Highlights:

- Intact lipids from sinking and suspended particles from two well-monitored ocean sites are assessed with semi-targeted methods.
- Changes in lipid compositions at both sites show non-polar triglycerides transfer better to depth than polar lipids.
- Saturated lipids appear to be preferentially incorporated during particle formation, based on patterns observed in a thylakoid-specific lipid class, but they do not appear to be preferentially preserved or transferred as particles sink.
- Two new metrics based on intact lipid compositions are used to track both the broad source of sinking material as well as the level of lipid degradation in material.

1.0 Introduction:

Earth's relatively small pool of atmospheric carbon is controlled by fluxes from much larger terrestrial and ocean reservoirs. In the ocean system, autotrophic phytoplankton fix carbon dioxide into biomass on a scale roughly equal to terrestrial production as estimated with satellite observations (Behrenfeld et al., 2001; Westberry et al., 2008). A portion of this biomass, and the fixed particulate organic carbon (POC) it contains, sinks out of the sunlit photic zone into the mesopelagic where it is re-mineralized or transits further still into the deep ocean (Martin et al., 1987). This downward flux of carbon is referred to as the biological carbon pump (BCP) and is

thought to be the major control on deep ocean CO_2 gradients (Sarmiento and Gruber, 2006). The BCP can be broken down into multiple sub-processes the largest of which is simply the gravity driven settling of POC in the water column (Boyd et al., 2019). This process, among other biologically mediated processes, is modeled to be the largest contributor to the ocean BCP worldwide (Nowicki et al., 2022). The BCP is critical for both sequestration of carbon as well as support of mesopelagic ecosystems (Iversen, 2023). Without the influence of the BCP on inorganic carbon inventories, it is estimated that the ocean would sequester 8% less carbon (DeVries, 2022).

Identifying biogeochemical factors affecting the rate, depth, and consistency of POC flux attenuation is important for a predictive understanding of the BCP. One such factor is the relative amount of sinking material derived from different particle types. Sinking particles can form in a variety of ways, however, most particles can be grouped into fecal pellets, large individual single cells, 'marine snow' aggregates, and zooplankton carcasses (Turner, 2015; Siegel et al., 2023). Fecal pellets derive from zooplankton grazing on phytoplankton, other zooplankton, or marine detrital particles. Aggregates can come from a wide range of sources but principally form via carbohydrate and protein rich extracellular polymeric substances (EPS) excreted by cells that coagulate into dense sinking particles (Passow, 2002). The relative importance of each of these particle types to the BCP is difficult to constrain but mechanistically relevant given their different formation pathways and possibly different physical-chemical properties (Boyd and Stevens, 2002; Laurenceau-Cornec et al., 2015; Omand et al., 2020). The mechanism of carbon remineralization is another critical factor for accurate characterization of the BCP. Direct solubilization and remineralization of carbon on marine particles by attached bacteria has long been thought to play an important role in sinking flux attenuation (Smith et al., 1992; Bidle and Azam, 1999). However, observations and modeling efforts have highlighted that other processes such as fragmentation are

likely also important in removing carbon from the fast sinking pool (Collins et al., 2015; Amaral et al., 2022). The extent to which remineralization of POC is, or is not, chemically selective during transit is unclear with ramifications for accurate representations of degradation processes (Hedges et al., 2001; Lee et al., 2004).

Examining the labile organic molecules that make up sinking POC can give insights into these BCP processes; of particular interest are glycerolipids – a group of relatively labile and chemically diverse organic soluble molecules (Van Mooy and Fredricks, 2010). Different profiles of glycerolipids are produced by bacteria and phytoplankton giving particulate glycerolipid compositions potential as a broad carbon source indicator (Popendorf et al., 2011). Additionally, glycerolipids have been used to examine degradation processes in marine settings as their compositions appear to be sensitive to remineralization processes (Goutx et al., 2003, 2007; Cantarero et al., 2024). Identifying individual organic 'biomarkers' that are predictive of POC sources and remineralization processes has been a goal in oceanography for decades (Wakeham et al., 1997). However, advances in mass spectrometry have allowed for a wider range of compounds to be measured within a single sinking POC sample (Fulton et al., 2017; Johnson et al., 2020; Hunter et al., 2021). This analytical progress allows reevaluation of existing paradigms in organic matter remineralization and development of new compositional indices.

In this study, we examine the glycerolipid composition of sinking and suspended POC using high resolution mass spectrometry during two ocean flux studies in the North Atlantic and North Pacific Ocean. We find the largest differences in sinking lipid compositions to be spatial and temporal; overall, we observed less dramatic compositional shifts with depth. We find a wide spectrum of glycerolipid transfer efficiencies but conclude that most of the glycerolipid mass must be lost via non-selective processes to best explain sinking compositions at mesopelagic depths.

While we do not observe major transfer efficiency differences based on lipid unsaturation, we do observe a partitioning between surface suspended material and sinking material pointing to a selection against unsaturated lipids during early mesopelagic particle formation. Using lipid compositions from single particles, we create a new compositional index that tracks the relative amount of fecal pellets versus aggregates in a sample based on glycerolipid abundances and validate this index with concurrent optical observations of particle compositions. We additionally show that this index is well correlated to the ratio of lipid metabolites and intact lipid species (i.e., hydrolysis index) pointing to zooplankton digestion as a large control on sinking material degradation at both ocean sites. Lastly, we evaluate these findings in the larger context of both flux studies and discuss their implications for our understanding of BCP mechanisms.

2.0 Methods:

2.1 Field Settings

We collected the field samples presented here as part of the 2018 and 2021 "EXport Processes in the Ocean from RemoTe Sensing (EXPORTS)" mission. Field campaigns were targeted at well-monitored ocean sites and separated into North Atlantic and North Pacific deployments (Fig. 1) with multiple ships participating in each. The first deployment (concurrent cruises RR1813 and SR1812 hereafter referred to as the "North Pacific" field site), was located near the Ocean Station P mooring site (50.1°N, 144.9°W) during August and September 2018. The second deployment (concurrent cruises JC214, SdG2105, and DY131 hereafter referred to as the "North Atlantic" field site), was located near the Porcupine Abyssal Plain Sustained Observatory (PAP-SO) mooring (49°N; 16.5°W) during May 2021.

Each campaign was separated into three sediment trap collection periods at the beginning of which sediment traps were deployed and at the end of which they were recovered. Lipid samples from

traps were not available during every sampling period and in some cases were collected but unusable (see section 2.3). Samples presented here derive from the third collection period of the North Pacific campaign (August 31st to September 5th 2018), the first collection period of the North Atlantic campaign (May 5th to 7th 2021), and the last collection period of the North Atlantic campaign (May 22nd to 25th 2021). For ease of description here, these three particle collection periods will be referred to as "North Pacific", "early North Atlantic", and "late North Atlantic". Suspended lipid sampling was taken throughout each deployment and are presented here unseparated by trap collection period. During the North Pacific campaign there was relatively little change in water column conditions, sinking particle compositions, and only a slight increase in sinking fluxes near the end of the cruise (Durkin et al., 2021; Estapa et al., 2021). As such our North Pacific sinking samples from the final sampling period are fairly representative for the deployment. However, the large changes in water column conditions between the beginning and end of the North Atlantic campaign created highly different states for the BCP between the early and late sampling periods. In depth descriptions of the oceanographic conditions of both sites during the course of each trap sampling period can be found in Siegel et al., 2021 and Johnson et al., 2024 respectively.

2.2 Sinking and suspended material collection

We collected sinking organic material on both cruises with surface-tethered traps (STT) as well as neutrally buoyant sediment traps (NBST). Methods for trap deployment, sinking material processing, and results of bulk elemental analysis are described in detail for the North Pacific campaign elsewhere (Estapa et al., 2021; Roca-Martí et al., 2021). Additionally, information on NBTS design as well as collection tube design can be found in (Estapa et al., 2020). Identical collection methods were used in the North Atlantic deployment. In brief, sinking material was

collected at multiple depths in two cylindrical polycarbonate tubes filled with 0.1% formaldehyde-poisoned brine and overlayed with 1-µm filtered seawater. Trap tubes collected sinking material at depth for 2-6 days, were sealed at depth, and recovered for analysis. Two trap lipids samples from the North Atlantic had anomalies during collection: the 75-meter trap sample from the early North Atlantic sampling period collected for double the time of other samples due to a lid closure malfunction. Additionally, the 500-meter trap samples from the late North Atlantic sampling period also failed to close and spent ~5 hours at the surface open where particles could be collected. While important to note, neither of these events appear to have compromised these samples as brine layers remained intact. Recovered material for elemental and lipid analysis was filtered through a 335-µm screen and picked clean of large zooplankton under a microscope. A splitter was used to divide the material into equal fractions: two tubes were combined and one eighth of the particles from the combined two tubes was filtered onto a pre-combusted quartz microfiber filter (QMA, 1 µm nominal pore size) for lipid analysis. These QMA filter types were chosen for lipid analysis to exactly match the filter type used for POC and other elemental analysis (Estapa et al., 2021).

Suspended particles for lipid analysis were collected during both deployments using Niskin bottles mounted on a CTD rosette. Samples were immediately collected from Niskin bottles and filtered onto 0.2 µm Durapore filters (Millipore Sigma, GVWP04700); one liter of seawater was filtered at all depths with the exception of two-liter samples taken below 330 meters depth at some time points. Additional one-liter samples for lipid analysis were taken from surface waters via the ships flowthrough system during the North Atlantic campaign. All filters for lipid analysis were flash-frozen in liquid nitrogen, transported via a dry shipper, and stored above liquid nitrogen in a dewar until lipid extraction.

2.3 Zooplankton Contamination

The majority of sinking samples from the North Pacific were highly impacted by non-sinking zooplankton entering trap tubes and perishing (i.e., 'swimmers'). Despite screening measures, microzooplankton and amphipod eggs smaller than the 335 μm screen impacted both POC and lipid samples. In order to estimate sinking POC with swimmers removed, unsupervised classification was used to identify a small subset of samples unlikely to be contaminated with swimmers (Estapa et al., 2021). Using this subset, the remaining POC values were corrected. To ensure that lipid samples of sinking material from the North Pacific were interpretable, we limited our analysis only to collected lipid splits that were part of this low-swimmer subset. There is, however, no quantitative estimate for swimmer contamination of these samples. For lipid samples this comprised four STT samples during the last sampling period of the North Pacific. Lipid sample fluxes used in our analysis were well correlated with finalized POC values derived from both field sites (Fig. 1G, $R^2 = 0.84$, $p < 0.001$).

2.4 Lipid Analysis

We used a modified Bligh and Dyer to obtain a total lipid extract from both sinking and suspended samples; methods for lipid extraction as well as mass spectrometry analysis were identical to methods used in Holm et al., 2022. Using these methods, we annotated 1,172 lipid species from the North Atlantic and 930 lipid species from the North Pacific, spanning variation in lipid class, fatty acid carbon number, and degree of unsaturation. These glycerolipids included membrane forming intact polar lipids (IPLs), energy storage triacylglycerides (TGs), as well as metabolic intermediates of these intact groups in the form of diacylglycerides (DGs), and monoacylglycerides (MGs). IPLs can further be separated by their headgroups into multiple membrane lipid classes of which we annotated 9 specifically. Abbreviations and full class names can be found in Supplementary Table 1 and match LIPID MAPs style. See Holm et al. 2022 for

full lipid class annotation information. The mean unsaturation for a whole lipid sample was calculated as described in Holm et al. 2022.

Quantification of lipid species was performed as described in Holm et al., 2024. Deuterated internal recovery standards for each class were used as described in Holm et al. 2024. In this paper, however, we calculated the limit of detection for each class by using pooled quality control samples rather than prediction intervals of standard curves (Supp. Fig. 1). This method takes advantage of the variability in concentrations of lipid species within the pooled quality control from each class. Using repeat measurements, we were able to model the probability we would detect a lipid species at a certain concentration. Similar to methods used in Armbruster and Pry, 2008, we set the LOD at the concentration of where we modeled that we would detect a lipid species 95% of the time.

Final lipid concentrations for each lipid species were field-blank corrected. North Pacific sinking-particle samples were blank-corrected by subtracting values measured in filtered brine from an undeployed trap tube. Suspended material was blank corrected with a 1L purified MilliQ water sample collected at sea in the same manner as suspended and treated identically in lab preparation. North Atlantic suspended samples and sinking samples were blank corrected with the mean lipid concentrations from four 1L MilliQ field samples taken at sea as a brine blank was not available. Blank correction on average decreased the total lipid abundance of a trap sample by 5%.

2.5 nMDS Analysis

We used nMDS ordination analysis from the R package ‘vegan’ to explore compositional similarities between our sinking and suspended lipid samples. We use quantified concentrations of lipids species present at both sampling sites (n = 735). Data was square root transformed and standardized before nMDS analysis. We ran two nMDS analysis, one with only sinking material

and one with sinking and suspended material combined. Lastly, we fit vectors of sample metadata to the nMDS ordination to test correlations between the sample compositions and various metadata.

2.6 Individual sinking particle training data for lipid source metric (LD_{LIP})

We applied linear discriminant analysis (LDA) to create a new biogeochemical index (LD_{LIP}) reflecting the relative fecal pellet and aggregate contributions to marine sinking material. The published lipid compositions of 31 individual sinking particles (both fecal pellets and aggregate particles) were used as training data to establish coefficients for our LDA index (Hunter et al., 2021). We then applied the index to bulk samples from both EXPORTS campaigns to evaluate the particulate sources contributing to sinking POC.

Full methods for single-particle lipid quantification can be found in Hunter et al., 2021. Briefly, individual sinking particles were isolated during a May 2017 cruise (AR16) in the North Atlantic on a transect between Bermuda and Woods Hole. Particles were collected at 150m in a surface-tethered conical net trap over a 24-hour period. The net traps contained no poison or brine as particles were also separately used for respiration experiments. Particles were imaged, manually classified, and isolated into a 96-well plate from sinking material by hand with a stereomicroscope and glass capillary for manipulation. After isolation, lipids were extracted using a microscale version of the Bligh and Dyer method (Hunter et al., 2021). Unlike for bulk-sample lipid analysis, a nanoflow high-performance liquid-chromatography system was used in tandem with the Q-Exactive orbitrap mass spectrometer to achieve quantification of low mass samples. Quantified lipid data for individual particles used in this study is available online (Hunter et al., 2021).

231 The mole fraction of lipid species comprising major glycerolipid classes (Supp. Table 2) from each
232 particle were used in the LDA training data. The percentage of individual lipid species were
233 grouped into lipid class totals creating 10 variables for the LDA. MGs were not assessed in
234 individual particles and were not included in the analysis. Input variables were square-root
235 transformed to improve variable linearity and standardized to insure equal weighting in the index.

236 We appreciated that aggregates in our training set likely contained a variable proportion of fecal
237 material within them. LDA is similar to PCA in that it generates a linear combination of variables
238 that can be used to reduce the dimensionality of a dataset. Indices based on linear equations such
239 as PCA and LDA can be calculated for any sample that contains all the variables used in initially
240 creating the index. Unlike PCA which creates metrics that capture the greatest variance between
241 variables, LDA finds a combination of variables that best separates two or more groups of samples;
242 in this case fecal pellets and marine snow aggregates. The presence of fecal material in aggregate
243 particles at first appears confounding, and would be for a mixing model approach where
244 endmember compositions are bounded. However, with LDA there are no bounds in either direction
245 on the new metric. Therefore, we can view the discriminant function as useful in tracking this
246 compositional change as long as there is considerable separation between the training sets in our
247 parameters of interest. In other words, we only need to assume that our individual aggregate
248 particles contain proportionally much less fecal material than our individual fecal pellets in order
249 to get a good metric for separation using our training data.

250 The particle source (LD_{LIP}) index for any sample can be calculated as:

251 $$LD_{LIP} = \sum_{i}^{n} \left[\frac{\sqrt{mole_i} - \mu_i}{\sigma_i} \right] \times \beta_i$$

where $mole_i$ is the molar fraction of the lipid class out of the training classes, u_i is the class mean from our square root transformed training data, σ_i is the class standard deviation of the square root transformed training data, and β_i is the modeled coefficient for said class using our single particle training data. Coefficients as well as the square root transformed mean and square root transformed standard deviation of training data for each variable can be found in Supplementary Table 2.

Without replicates of our sinking material from EXPORTS campaigns it was not possible to determine the precision of this index in field samples via replication. The mean and standard deviation of LD_{LIP} in 67 replicate quality control samples was 1.68 ± 0.048 indicating a small standard deviation just from analytical error (Supp. Fig. 2A). Additionally, the relative standard deviation of the mole percentages of the nine lipid classes in the quality control samples varied between 2.4% to 6.2%. Based on these values, we used a Monte Carlo simulation to estimate the error in individual sinking samples. We allowed each of the underlying mole percentages to vary on a normal distribution with a relative standard deviation of 10%. We used approximately double the observed relative standard deviation value than was observed in quality controls for each mole percentage to attempt to incorporate error from sample extraction and handling. We used 1000 simulations where mole percentages were drawn at random from these normal distributions and calculated the standard deviation of resulting LD_{LIP} values for each sample. Standard deviation of the index in EXPORTS samples using this method ranged from ±0.133 to ±0.178.

2.7 Modified Lipid Hydrolysis Index Calculations (LI_{MOD})

Goutx et al., (2003) proposed a hydrolysis index (also referred to as 'lipolysis') that captures the relative levels of lipid metabolites to the proportion of intact lipid species. We calculated a modified version of this index as:

$$LI_{MOD} = log10\left(\frac{DG + MG}{IPL + TG}\right)$$

where DG, TG, MG, and IPL are the moles of each respective lipid class in a sample. We excluded fatty-alcohols and wax esters from this ratio because the method used here cannot detect them. Additionally, we added betaine lipids to the denominator as part of IPLs as they represent membrane lipids similar to phospholipids and glycolipids that could yield products in the numerator upon degradation. Lastly, we used a log-scale to linearize the ratio and facilitate comparison to other metrics. It has been noted that calculating the mean or performing linear regression using un-transformed stoichiometric ratios can produce somewhat biased results particularly based on selection of the denominator (Isles, 2020). To avoid such pitfalls, we use log-transformation or log scales for ratios in this analysis. We estimated analytical error for this metric in sinking material based on the relative standard deviation of quality controls.

2.8 Carbon flux determination from gel traps

We compared our lipid indices to the carbon flux from particle types within trap material from both deployments as assessed by optical methods. A non-poisoned third tube containing a polyacrylamide gel was located on each platform to assess flux magnitude and composition via imaging. Gel trap method design, sample collection, and flux modeling of samples from both field sites has been published elsewhere (Durkin et al., 2021; Bodel et al., 2025). More information on this gel imaging, processing, particle categorization, and carbon flux modeling for both cruises can be found in Bodel et al. 2025. Briefly, gels were placed in the bottom of trap tubes and overlayed with 1 μm filtered seawater. After settling of particles during deployment and trap recovery, gels were imaged at four increasing magnifications. Individual particles were detected within the images via a series of image transformations. Particle identities were assigned to each identified

particle by manually screening images. Notably, particle size limited identification; particles smaller than 40 μm were identifiable only half of the time in Pacific data (Durkin et al., 2021). After particles were classified, estimates of their width, volume, and length were determined from the equivalent spherical diameter. Published relationships between volume and carbon were used to assess carbon fluxes from each particle class and for samples as a whole. Only identified particles were included in calculations of carbon flux.

For comparison with lipid indices, using quantified optical POC flux data from Bodel et al., 2025, we calculated the ratio of carbon flux from aggregates versus fecal pellets. Rhizaria and individual phytoplankton cells were not included in the calculation. Image categories varied slightly across Pacific and Atlantic deployments and were handled in the following way: Pacific data broke fecal pellets into more subgroups than Atlantic classification; all groups identified as fecal were included in the denominator. Lastly, image identifications of aggregates from the Pacific were further subset into "dense detritus" which we grouped with aggregates in our calculation. Error, as determined in Bodel *et al.* for optical POC fluxes, was propagated into the final ratios via first-order Taylor series method (Ucar et al., 2018).

3.0 Results

3.1 Sinking glycerolipid flux profiles showed compositional differences across basins

Sinking fluxes of pooled glycerolipid classes displayed similar patterns across oceans and sampling periods with certain exceptions (Fig. 1). Despite variable flux patterns on a lipid species level, when grouped to the lipid class level, most classes showed rapid attenuation with depth (Fig. 1A-E). A notable exception to this trend of decreasing flux appeared in the late North Atlantic sampling period during which there were larger fluxes and greater proportions of marine snow

aggregates compared to other deployments. During the late North Atlantic sampling, overall fluxes of DGs increased continually with depth (Fig. 1B). Glycerolipids flux as a percentage of bulk POC ranged from 1-3.9% across both deployments (Fig. 1G). Bulk POC flux was well linearly correlated to lipid flux with slope of 1.6% for the relationship across all three epochs ($R^2 = 0.84$, $p < 0.001$). No significant correlation between glycerolipids flux as a percentage of bulk POC and depth was observed across combined deployments (Spearman's rank correlation, $p = 0.16$) with also no significant difference between deployments in this percentage (Krustal-Wallis test, $p = 0.51$).

Across all three sampling periods, TGs and IPLs together made up the majority of glycerolipid flux at all depth horizons (mean of 87%, range of 80-92%) with glycerolipid metabolite species (DGs and MGs) making up a smaller but persistent fraction of the flux (Fig.2). Individually, TGs and IPLs made up a remarkably similar proportion of sinking material; TGs made up 44% of glycerolipid flux on average (range of 29-54%) while IPLs made up 43% (range of 30%-54%). There were, however, persistent compositional changes between these two groups with depth. Looking at all three sampling periods combined, the proportion of IPLs out of total glycerolipids was negatively linearly correlated with depth ($R^2 = 0.63$, $p < 0.001$) while the TG fraction was positively linearly correlated with depth ($R^2 = 0.44$, $p < 0.05$) pointing to a persistent increase in the relative amount of TGs with depth. Between the three sampling periods, the amount of glycolipids differed (Fig. 2), owing almost entirely to changes in the amount of sulfoquinovosyl diacylglycerol (SQDG), a lipid class sourced from photosynthetic cells (Goddard-Borger and Williams, 2017). SQDG lipid levels as a percentage of IPLs were significantly different between sampling periods (Fig. 2D-F, Krustal-Wallis test, $p < 0.01$). SQDG as a percentage of IPLs from the North Atlantic were significantly elevated over North Pacific and significantly increased

during the North Atlantic campaign (Wilcox test, all $p < 0.05$). This result could point to an increased fraction of photosynthetically derived material in the North Atlantic especially near the end of the cruise.

We used nMDS analysis of lipid compositions to further examine the driving patterns behind lipid flux compositions in suspended and sinking material with depth (Fig. 3). When just the sinking material was analyzed on its own without the suspended data, three distinct groups formed corresponding to sampling period (Fig. 3A). We tested vectors of bulk properties of the sinking samples. Testing included POC, particulate inorganic carbon (PIC), biosilica (bSi), total nitrogen (N), and collection depth to see if lipid compositions were related to any of these. Three metadata vectors examined were significantly correlated to the sinking nMDS projection; PIC:POC ratio, bSi flux and the absolute POC flux concentrations ($p < 0.05$). Notably, trap collection depth was not significantly correlated as a vector ($p = 0.46$) implying it is not the major organizing factor for lipid compositions among sinking material as compared to sampling period.

We further examined our sinking material combined with suspended samples from both ocean deployments (Fig. 3B). Suspended material separated into two groups corresponding to the North Atlantic and North Pacific sites. After this, suspended samples separated based mostly on depth with a continuous gradient across samples. In this combined analysis we found that sample collection depth was significant as a vector ($p < 0.01$). Sinking material clustered separately from suspended with small separation corresponding to sampling periods. Despite being collected concurrently from the same depth range as suspended material, sinking material did not distribute in the same direction with depth and instead clustered closer to shallower suspended material. Thus, while suspended material saw large shifts with depth, the sinking material was comparatively static, and closer in composition to surface material.

364 3.2 Glycerolipid Transfer Efficiencies

365 We calculated the transfer efficiency for each lipid species (T_{eff}) from the first depth of each sinking
366 profile to each successive depth in that profile. We only considered T_{eff} from within continuous
367 platform types (i.e., NBST or STT). We additionally calculated the T_{eff} of each lipid class as a
368 whole and all glycerolipids combined (Supp. Fig. 3). To illustrate the diversity of lipid T_{eff} within
369 groups we present the T_{eff} of the entire lipid class alongside the 75^{th} and 25^{th} percentile T_{eff} of
370 individual lipid species within that group as error bars (Supp. Fig. 3).

371 The T_{eff} of the total glycerolipids mass was greater or close to the T_{eff} of POC for all North Atlantic
372 depth horizons (Supp. Fig. 3). In the North Pacific, total glycerolipids T_{eff} was above POC T_{eff} in
373 the surface and lower than POC for the 100m to 330m and 100m to 500m depth horizons (Supp.
374 Fig. 3). As with POC, the T_{eff} of the total glycerolipid flux tended to decrease with depth. On an
375 individual lipid species level, T_{eff} was widely distributed including lipid species that increased their
376 flux with depth and those that completely disappeared at depth. Out of 659 lipid species detectable
377 in sinking material of both campaigns, 96 species had a T_{eff} to 500m consistently in the bottom
378 50% of lipids across all sampling periods. These consistently poorly transferred lipids were diverse
379 and contained species from all detectable classes (Supp. Fig. 4). An additional 141 lipids
380 consistently had a Teff to 500m in the top 50% of lipids (Supp. Fig. 4). This group was much less
381 diverse and consisted of 115 TGs, 12 MGs, and 14 IPLs. This higher T_{eff} of some TGs can be seen
382 in the compositional changes of lipid classes with depth (Fig. 2). Given this observation of high
383 T_{eff} TGs, we tested whether the class as a whole had significantly higher T_{eff}. We found that on a
384 pairwise basis, TGs transferred to depth better than non-TG glycerolipids (Paired t-test, $p = 0.038$,
385 Supp. Fig. 3). However, while elevated over the T_{eff} of POC at many depth horizons, TGs did not

386 have a significantly higher T_{eff} than POC on a pairwise basis (Paired t-test, $p = 0.073$, Supp. Fig.
387 3).

388 3.3 Changes in sinking lipid saturation with depth

389 Unsaturated lipids, in particular, are thought to be more susceptible to degradation during organic
390 matter diagenesis. We therefore examined whether lipid unsaturation in sinking particles changed
391 with depth. The unsaturation level of IPLs and TGs were both generally invariant over the 500-
392 meter depth range surveyed in all three sampling periods (Supp. Fig.5). No sampling period
393 showed the hypothesized large decrease in unsaturation with depth despite large attenuations in
394 the combined IPL or TG lipid flux over 500 depth range in every sampling period (Supp. Fig. 5).

395 The SQDG polar lipid class provides a unique set of biomarkers for isolating the effects of selective
396 degradation on unsaturation as well as the interplay between sinking and suspended material.
397 SQDG is a unique component of thylakoid membranes that is understood to be produced
398 exclusively by photosynthetic organisms in the ocean (Van Mooy et al., 2006; Popendorf et al.,
399 2011; Goddard-Borger and Williams, 2017). As such, below the photic zone, there should be no
400 production of it by microbes and any changes in the suspended or sinking SQDG pool saturation
401 state can be understood to come only from remineralization of phytoplankton. We plotted the mean
402 number of unsaturations per SQDG fatty acid versus depth in both suspended and sinking material
403 for both deployments (Fig. 4). Additionally, we predicted the mean number of unsaturations that
404 SQDG would have based only on the water temperature alone at each depth. This utilized a
405 previously published relationship found between water temperature and SQDG in mixed layer
406 suspended samples (Holm et al., 2022). Notably, suspended material from the North Pacific study
407 site was included in establishing this linear relationship while the North Atlantic site was not.

In the North Pacific, mean SQDG saturation in suspended material tracked our temperature-based prediction within the 95% prediction intervals until just below the base of the euphotic zone. Deeper than this, suspended material unsaturation decreased and developed considerable spread. Sinking material was more unsaturated and closer in value to photic zone suspended material at 100m depth before quickly decreasing in unsaturation at 150 meters and staying largely invariant with a slight decrease in unsaturation to 500m. Suspended material from the North Atlantic followed largely the same trend as suspended material from the North Pacific: samples centered around our prediction until approximately 100 meters depth when it shifted to more saturated. Sinking material in both North Atlantic sampling periods was largely invariant with depth and positioned just outside the or on the edge of the 95% confidence interval from our temperature prediction.

3.4 New index (LD_{LIP}) generated from single particle data can separate particle types with lipids

Our model trained with individual sinking particles yielded good separation of individual fecal pellets and aggregate particles with a single linear function (Supp. Fig. 2A). While there was some overlap between the two groups of single particle training data in the index, their distributions were significantly different with aggregate particles being more positive on the index (Kruskal-Wallis, $p < 0.001$, Supp. Fig. 2A). Standardized coefficients of the LD_{LIP} index revealed the lipid classes that best separated particle type in the single particle training data; PE, MGDG, DGCC, and DG were weighted toward fecal pellets (negative) while SQDG and PG were most associated with aggregates (positive, Supp. Table 2). In addition to standardized coefficients, we examined the correlations between the index and original variables to assess influence (Supp. Fig. 2B). Of the nine lipid classes, in addition to high positive weights, molar percentage of PG in training data

was most positively correlated with LD_{LIP} (Spearman correlation, R = 0.82, $p < 0.001$). DG was significantly negatively correlated with LD_{LIP} (Spearman correlation, R = -0.45, $p = 0.011$).

3.5 Changings in sinking particle degradation and fecal level via lipids

We applied our source index (LD_{LIP}) and modified degradation index (LI_{MOD}) in EXPORTS trap material comparing it to depth, bulk elemental compositions, and optical assessments of particle compositions (Fig. 5). Profiles of LD_{LIP} reflected some changes in sinking particle composition with depth with most change occurring in the late North Atlantic sampling period (Fig. 5A). LD_{LIP} was significantly lower in North Pacific samples than North Atlantic samples (Wilcox test, $p = 0.01$) implying a more fecal composition. In STT samples from North Pacific, LD_{LIP} decreased toward a more fecal composition at 500 meters but was largely invariant at other depths. LD_{LIP} was elevated in STT samples from the early North Atlantic over the North Pacific (i.e., more aggregate particles), with little change with depth. Interestingly, one NBST samples from the 175 meter depth during the early North Atlantic sampling was higher than all STT samples from this period with the 175 meter STT largely matching the other NBST sample. This implies that this NBST was collecting more aggregate material than the other traps. While the entire profile was not significantly different from the early North Atlantic sampling, samples from the late North Atlantic displayed the highest measurements of LD_{LIP} we observed in sinking material indicating a high aggregate percentage. While increasing slightly from 100 meters to 200 meters during late North Atlantic sampling, the index decreased rapidly at 330 meters and 500 meters to within the range of the early sampling period implying more fecal particles at depth.

LD_{LIP} was well correlated to the relative flux of aggregates and fecal pellets as assessed by imaging gel traps ($R^2 = 0.61$, $p = 0.003$) when a single notable outlier was removed (Fig. 5C). Our lipid source index LD_{LIP} and gel trap optical flux had large disagreements on the 500m sample from the

late North Atlantic with the lipid data implying more fecal pellets than were observed. However, gel trap imaging corroborated some subtle differences in particle lipid composition observed in our LD_{LIP} index. Notably, the NBST at 175 meters from the early North Atlantic collected more carbon from sinking aggregates that fecal pellets according gel imaging. Additionally, the other NBTS also at approximately 175 meters during the same sampling periods collected less carbon from aggregates than fecal pellets. Our metric also reflected this difference in collected material during the same sample period.

We used LI_{MOD} to track the relative hydrolysis state of glycerolipids (Fig. 4-5C). Given the relatively fast turnover time of glycerolipids, it is best to interpret this metric as a tracker of current or highly recent (hours to days) remineralization of glycerolipids (Goutx et al., 2003). Unlike with the LD_{LIP} index, the three sampling periods were less clearly separable. In the North Pacific and late North Atlantic period, hydrolysis state decreased slightly over the first 50-100 meters below the photic zone before increasing steadily up to 500 meters (Fig. 5B). Much like our lipid source index, LI_{MOD} was comparatively invariant with depth for the early North Atlantic sampling with the NBST samples at 175m again representing extremes for hydrolysis level.

Our particle source index (LD_{LIP}) was linearly negatively correlated with our modified lipid degradation index (LI_{MOD}) implying that more fecal pellet heavy samples were richer in hydrolyzed lipids than aggregate heavy samples (Fig. 5D, $R^2 = 0.53$, $p < 0.01$). Similarly, our LI_{MOD} index was significantly correlated with gel trap aggregate to fecal flux ratios (Fig. 5E, $R^2 = 0.62$, $p < 0.01$) when the 500m late North Atlantic sample with large compositional disagreement was again excluded.

Lastly, we compared our two-lipid metrics to elemental ratios in the bulk trap material (Supp. Fig. 6). These include the particulate inorganic carbon to particulate organic carbon ratio (PIC:POC) and bio-silica to particulate organic carbon ratio (bSi:POC). Ratios between PIC:POC and bSi:POC can be viewed as the average level of mineral ballasting present in sinking material. LD_{LIP} was positively correlated with bulk PIC:POC (Spearman Rho = 0.59, p = 0.024) and LI_{MOD} was negatively linearly correlated (Spearman Rho = -0.63, p = 0.014). Neither lipid index was significantly correlated to bSi:POC or N:POC.

4.0 Discussion

4.1 Lipid fluxes show signs of food web and system state at both sites

Lipid fluxes from the Pacific and Atlantic EXPORTS campaign derive from two ocean sites under largely different biogeochemical states. A large food web analysis co-occurring with our study of the North Pacific study site revealed a highly detrital and zooplankton dominated food web where the majority of sinking carbon could be attributable to mesozooplankton and salp fecal pellets (McNair et al., 2023). Additionally, nitrogen stable isotope analysis of the North Pacific site revealed that these zooplankton consumers contributing most to export were likely 3rd to 4th order consumers (Shea et al., 2023). This disconnection of exported material from primary production can be seen in the composition of sinking IPLs where very few phytoplankton membrane glycolipids remain relative to the other sampling periods (Fig. 2). At the North Atlantic site, especially the later sampling period, a much higher SQDG fraction was observed implying a much tighter connection to primary production within sinking carbon during this period. Net primary production measurements from both deployments showed much higher rates of photic zone primary production overall in the North Atlantic as well as a greater fraction of this production

derived from large cells (Meyer et al., 2022, 2023); a tighter net primary production-to-export link appears to affect not just flux levels but organic composition differences between the sites.

The overall contribution of lipids to sinking organic matter is highly variable across ocean studies and may also be a product of photic zone environmental state. Our values of 1 to 3.9% glycerolipids are consistent with flux percentages previously observed in the North Atlantic (Fulton et al., 2017). While this study did not quantify fluxes of TGs, assuming an approximate 1:1 ratio between IPLs and TGs as we observed at both sites brings their values more in-line with ours. These percentages are lower than values reported for total lipid flux percentages (which includes lipids other than glycerolipids), in other ocean provinces and seas (~10%, Wakeham et al., 1997; 9-28% Goutx et al., 2000). In areas with little nitrogen or phosphorus stress, accumulation of excess energy storage lipids by phytoplankton is unlikely to be as advantageous compared to nutrient limited zones. As such, glycerolipids possibly represent a greater proportion of export from areas under different growth limitation dynamics.

4.2 Remineralization processes and lipid transfer efficiencies

Our methods were able to capture a wide spectrum of lipid transfer efficiencies on a molecular level. The glycerolipid pool as a whole tended to have slightly higher transfer efficiencies than bulk POC (Supp. Fig. 3) which was driven by a smaller subset of abundant lipids, many of which were TGs. Comparisons with POC transfer efficiencies illustrated that 45%-75% of lipid species had transfer efficiencies higher than POC over shallow depth intervals which dropped to 18%-55% for lipids at 500 meters. In both ocean basins, glycerolipids appeared to represent a 'moderately' labile pool of organic compounds; Previous studies have placed lipids in this middle zone of lability; macromolecular comparisons from Wakeham et al. 1997 showed lipids disappeared slower than pigments but faster than carbohydrates and proteins. Incubation experiments of sinking

521 particles in Goutx et al., 2007 additionally found the average lipid degradation rate was higher than
522 the protein pool.

523 Molecular-specific transfer efficiencies were highly dependent on location and sampling period,
524 however we observed that TGs as a class had significantly higher transfer efficiencies than other
525 glycerolipids. This also appears in both the lipid fraction of TGs with depth as well as in
526 consistently high specific transfer efficiencies where TGs were overrepresented (Fig. 2, Supp. Fig.
527 3). Other studies have noted that TGs represent an outsized portion of sinking glycerolipid mass
528 which could be the result of this high transfer efficiency (Bent et al., 2024). Reasons for this could
529 be both biological and physical. Recent work has shown that marine particle associated microbes
530 are selective degraders of certain lipid pools, and some lack the ability to degrade TGs (Behrendt
531 et al., 2024). It is possible that colonization of particles by TG degrading microbes is slower
532 compared to other degraders. Difference between these pools could result from their physical
533 locations within cells; lipids composing cell membranes may be exposed to external enzymes and
534 abiotic degradation more rapidly while TGs may be initially harder to access inside cellular lipid
535 bodies.

536 Despite these consistent patterns in remineralization with TGs being preserved, it is notable that
537 the largest lipid compositional changes across the sinking dataset tracked sampling period rather
538 than depth. In our nMDS analysis based on lipid composition, samples clustered by sampling
539 period rather than depth horizon and depth was not a statistically significant variable when
540 comparing metadata to the projection of sinking compositions (Fig. 3A). Class level compositions
541 shifted very little over material transit (Fig. 2).

542 From all of this, there are two conclusions to be drawn about remineralization processes in sinking
543 material collected by traps during both EXPORTS deployments. First, the initial epipelagic source

of sinking organic matter is a larger control on composition than remineralization processes at depth (Fig. 2, Fig. 3). Second, losses of sinking organic matter must largely be accomplished by non-selective mechanisms to explain lipid compositions. Fragmentation of large particles into small non-sinking particles or dissolved organic matter is one possible non-selective mechanism for lipid loss from large sinking material. In such a scenario, selective degradation processes may still predominate among lipids found in suspended phase. Indeed, as illustrated in our nMDS analysis, suspended material saw much greater transformations toward a similar composition with depth than sinking material did (Fig. 3). Assessment of amino acids in the North Pacific deployment further confirm a relatively uniform degradation state of large particles and depth associated changes in small particles (Wojtal et al., 2023). While no direct observations of sinking speed are assessed here, much of this dynamic may have to do with relative age of sinking versus suspended material. On average, sinking material may transit to depth in a matter of days to weeks (DeVries and Weber, 2017). Fragmentation in suspended particulate material should halt transit and allow time for selective remineralization to take hold. Many recent studies using multiple observational approaches have highlighted the importance of fragmentation as a sinking POC loss process (Collins et al., 2015; Briggs et al., 2020; Amaral et al., 2022). Experimental comparisons between water-column and on-particle respiration rates in the North Atlantic have suggested that direct respiration of sinking material on particles was a smaller loss process than other factors (Collins et al., 2015). Additional modeling of particulate concentrations during the North Pacific campaign has also implicated disaggregation as the major loss process for large sinking material during this study (Amaral et al., 2022).

Unsaturation in sinking material did not shift dramatically along its transit to 500 meters in any sampling period (Supp. Fig. 5). This finding is inconsistent with previous ocean flux studies that

report an increasing proportion of saturated lipids with depth in fluxing material interpreted as a result of different degradation rates of saturated and unsaturated lipids (Wakeham et al., 1997). There may be multiple explanations for the different findings in our study. Importantly, during both EXPORTS campaigns suspended lipid material from CTD samples saw dramatic decreases in overall fatty acid unsaturation level with depth. If traps in other studies were to collect smaller slower sinking particles over longer time intervals the contents may be more saturated than what we observed. Additionally, wax esters, which unfortunately could not be detected by our methods, may represent a highly saturated and non-labile endmember for fatty acids in traditional GC/MS based lipid analysis.

The mean unsaturation of SQDG in sinking material, which can be interpreted to only reflect degradation processes, further highlights several interesting conclusions about lipid remineralization (Fig. 4). First, at both sites, sinking SQDG was more saturated relative to mixed layer suspended material and, other than the shallowest sample from the North Pacific, began that way. This implies that selection mechanisms against unsaturated lipids are at play but occur close to sinking material's initial exit from the photic zone during particle formation. Second, it is notable that both suspended and sinking SQDG lipids strongly depart from the predicted unsaturation based on temperature outside the photic zone, a trend slightly clearer in the North Pacific. Intact membrane lipids have historically been interpreted as only deriving from living cells in the environment, given evidence of fast degradation in experiments (Harvey et al., 1986; Moodley et al., 2000). Our results here suggest that IPL-containing phytoplankton sinking below the photic zone here must, at a minimum, no longer be chemically maintaining their photosynthetic membranes and very likely are dead. This result adds observations on top of theoretical

589 calculations of the possible detrital fraction of IPLs in the mesopelagic but future work may
590 address this question more explicitly (Schouten et al., 2010; Gašparović et al., 2016).

591 4.3 Relative flux of different particle types is trackable by glycerolipid compositions

592 Principle component analysis (PCA) has been widely used in geochemistry and oceanography to
593 create descriptive indices to track organic matter degradation processes (Xue et al., 2011). When
594 calculated consistently, compositional indices such as these are statistically quantitative and can
595 be compared to other organic matter properties for both validation and prediction outside of
596 organic composition. Indeed, compositional indices that can be quantitatively linked to other
597 properties have found the most purchase; an amino acid degradation index based on PCA presented
598 in Dauwe et al., 1999 was shown to be directly linked to organic matter reactivity and has proved
599 highly valuable for tracking degradation processes in the ocean (Van Mooy et al., 2002; Wojtal et
600 al., 2023). Lipid compositions have been used extensively as qualitative biomarkers to examine
601 the influence of bacterial and zooplankton influence on sinking material (Wakeham and Canuel,
602 1988; Sheridan et al., 2002). Advances in ocean optics and modern mass spectrometry present an
603 opportunity to directly and quantitatively link organic matter compositions to these more
604 deployable optical monitoring strategies.

605 Our LDA-based compositional index for particle type (LD_{LIP}) showed that aggregates and fecal
606 pellets could be separated into distributions by their glycerolipid composition alone (Fig. 5). It is
607 worth emphasizing that this index was trained using aggregates collected from sinking material as
608 an end member, not the lipid compositions of phytoplankton. This is notable because the lipid
609 compositions of marine snow aggregates likely result from the totality of internal particle
610 conditions, not just an increased proportion of phytoplankton cells. The proportion of SQDG,
611 which derives only from phytoplankton, was weighted toward aggregates in our LDA model.

612 However, the high weighting of PG towards aggregates implies our model may also be tracking a
613 higher proportion of live bacteria in exopolymer-rich aggregate particles. PG is a variable (and
614 usually minor) component of photosynthetic membranes but also can be sourced largely from
615 heterotrophic bacteria in ocean water columns (Popendorf et al., 2011).

616 Our source metric largely aligns with concurrent observations during both EXPORTS campaigns.
617 Mixing models predicting sinking material source based on amino acid measurements at the North
618 Pacific site also found that sinking particles derived almost entirely from fecal pellets with little
619 depth variation (Doherty et al., 2021; Wojtal et al., 2023). The strong correlation between our LD_{LIP}
620 index and gel trap particle ratios has implications for both measurements (Fig. 5C). The correlation
621 implies that the lipid composition of fecal pellets is generally similar enough in glycerolipid
622 composition as to not disrupt the relationship. In traps, multiple distinct groups of fecal pellets
623 were identified and likely sourced from different groups of zooplankton consuming different prey.
624 Despite this, digestion appears to impart a consistent enough signal onto fecal pellets to be
625 identified in the glycerolipid pool and implies this index will be useful regardless of fecal pellet
626 origin. However, deviation between optical assessment and LD_{LIP} at 500m of the late North
627 Atlantic sampling period may indicate that our metric is most useful from approximately 100-350
628 meters where sinking aggregates have undergone minimal reworking. Validating this index in other
629 environments as well as development of metrics based on other organic molecule compositions
630 using the statistical approach here is likely to be the object of future work.

631 4.4 Zooplankton digestion is likely a major contributor to relative lipid hydrolysis (LI_{MOD}) in
632 both deployments

633 Goutx et al., 2003 first suggested that the ratio of lipid metabolites and intact lipids could be used
634 to track remineralization processes of lipids; in incubations of dissolved TGs with seawater

635 bacteria the authors observed DGs, MGs, and fatty acids metabolites all spiking relative to the
636 initial TG concentrations. While these lipid metabolites are in turn drawn down, this metric can
637 track the relative level of hydrolysis and highlight samples of active degradation. In further studies,
638 live incubations of sinking particles also increased abundance of these lipid metabolites overtime
639 (Goutx et al., 2007).

640 Hypothetically, this active degradation signal comes from hydrolysis of intact lipids by
641 extracellular lipases released by bacteria or within zooplankton guts. Hydrolytic enzymes
642 including lipases are released on sinking particles by bacteria during colonization (Smith et al.,
643 1992; Arnosti, 2011; Krupke et al., 2016). While not shown for glycerolipids specifically, a
644 mismatch between hydrolysis of large molecules and uptake of resulting metabolites has been
645 described in multiple ocean systems which could explain the accumulation of lipid metabolites
646 relative to intact species (Arnosti et al., 1994; Pantoja et al., 2009; Arnosti, 2011). Recent genomic
647 evidence examining phospholipid degradation by ocean bacteria implies that cleaving of the
648 headgroup moiety occurs extracellularly with specific transporters for phospholipid headgroups
649 on the cell surface (Westermann et al., 2023). Transit through a zooplankton gut in turn exposes
650 lipids to digestive lipases.

651 The correlation between our degradation (LI_{MOD}) and source (LD_{LIP}) index provides evidence that
652 zooplankton digestion is a major source of this active lipid hydrolysis and likely bulk carbon
653 degradation on sinking particles at both study sites (Fig. 5D). While zooplankton digestion appears
654 to play a large role in predicting recent hydrolysis, a good portion of this variability in LI_{MOD}
655 remains unexplained (R^2 = 0.53). This leaves room for other hydrolytic processes such as
656 aforementioned on-particle bacterial enzymatic degradation as well as differential protection of
657 labile material within particles.

5.0 Conclusion

A better understanding of the BCP will be critical for properly quantifying the effects of climate change on the carbon cycle and associated feedbacks. The needs surrounding this are twofold: 1) a more mechanistic understanding of BCP components and 2) more environmental datasets to evaluate and check our understanding. Highlighting the most critical factors for remineralization dynamics on a molecular level will allow us to understand how flux may (or may not) change in a warming ocean. Additionally, development of new geochemical datasets that can directly check our predictions around flux composition should also play an important role.

The work presented here has made progress toward both of these larger goals. We utilized a lipidomics approach to examine sinking and suspended lipids within particulate carbon from two well-studied ocean sites. By characterizing thousands of compounds from different sources we were able to track large-scale patterns in remineralization. We found that in both ocean sites, remineralization of sinking lipid matter was mostly non-selective – while lipids pools lost chemical diversity as they transited to depth there were few consistent patterns on a lipid species level. Long standing knowledge on the relative lability of unsaturated versus saturated lipids did not appear to impact remineralization in sinking material. This indicates that selective remineralization forces are more likely to play a larger role if sinking material becomes resuspended.

Additionally, using broad lipid classes, we developed a new metric (LD_{LIP}) to track the relative proportions of particle types in sinking material. Our metric captured the relative dominance of fecal material in flux at the North Pacific study site and additionally captured the dynamic aggregate driven event near the end of the North Atlantic campaign. Validation of this source metric by optical data from the EXPORTS collaboration points to its utility across ocean regions. Moving forward, examination of this metric with a larger more global collection of sinking

samples should prove useful for comparison to model predictions. Further development of lipid geochemical indices with modern analytical tools will continue to aid spatial and temporal characterization of the BCP.

Acknowledgements: This work was funded by a grant to the National Science Foundation (NSF) to Benjamin A. S. Van Mooy (OCE Award #1756254). We would like to thank the entirety of the EXPORTS science and planning team, including both at-sea and shoreside individuals who made the field campaign possible. We would like to thank the captains and crew of *R/V* Roger Revelle, *R/V* Sally Ride, *RRS* James Cook, *R/V* Sarmiento de Gamboa, and *RRS* Discovery across which all data presented here was collected. From the EXPORTS collaboration, we additionally would like to thank Dr. Margaret Estapa (University of Maine) who provided us with splits of sinking material for lipid processing and advised on interpretation of sinking fluxes. We would like to thank Dr. Colleen Durkin (MBARI) for collection of, and assistance in, interpretation of particle fluxes from gel traps on this campaign. Lastly, we would like to thank Dr. Ken Buesseler (WHOI) who read and offered feedback on a preliminary version of this manuscript. We would like to thank Dr. Alyson Santoro (UCSB) and Dr. Peter Morton (Texas A&M) for collecting suspended lipid samples during the RR1813 cruise at sea.

CRediT Statement: Henry C Holm: Data curation, Formal Analysis, Investigation, Methodology, Visualization, Writing – original draft, Writing – review & editing; Helen F Fredricks: Investigation, Methodology, Writing – review & editing; Benjamin A. S. Van Mooy: Conceptualization, Funding acquisition, Project administration, Resources, Supervision, Writing – review & editing

Data Availability: All quantified lipid data presented here can be found on GitHub (github.com/hholm/EXPORTS_lipids, v1.0.1) and Zenodo (doi.org/10.5281/zenodo.21298933).

Data for bulk fluxes for both cruises can be found on SeaBass (doi.org/10.5067/SeaBASS/EXPORTS/DATA001). Modeled aggregate and fecal pellet fluxes from gel traps can be found on Zenodo (doi.org/10.5281/zenodo.15446685).

References:

Amaral, V.J., Lam, P.J., Marchal, O., Roca-Martí, M., Fox, J., Nelson, N.B., 2022. Particle cycling rates at Station P as estimated from the inversion of POC concentration data. Elementa: Science of the Anthropocene 10, 00018. https://doi.org/10.1525/elementa.2021.00018

Armbruster, D.A., Pry, T., 2008. Limit of Blank, Limit of Detection and Limit of Quantitation. The Clinical Biochemist Reviews 29, S49–S52.

Arnosti, C., 2011. Microbial Extracellular Enzymes and the Marine Carbon Cycle. Annual Review of Marine Science 3, 401–425. https://doi.org/10.1146/annurev-marine-120709-142731

Arnosti, C., Repeta, D.J., Blough, N.V., 1994. Rapid bacterial degradation of polysaccharides in anoxic marine systems. Geochimica et Cosmochimica Acta 58, 2639–2652. https://doi.org/10.1016/0016-7037(94)90134-1

Behrendt, L., Alcolombri, U., Hunter, J.E., Smriga, S., Mincer, T., Lowenstein, D.P., Yawata, Y., Peaudecerf, F.J., Fernandez, V.I., Fredricks, H.F., Almblad, H., Harrison, J.J., Stocker, R., Van Mooy, B.A.S., 2024. Microbial dietary preference and interactions affect the export of lipids to the deep ocean. Science 385, eaab2661. https://doi.org/10.1126/science.aab2661

Behrenfeld, M.J., Randerson, J.T., McClain, C.R., Feldman, G.C., Los, S.O., Tucker, C.J., Falkowski, P.G., Field, C.B., Frouin, R., Esaias, W.E., Kolber, D.D., Pollack, N.H., 2001.

Biospheric Primary Production During an ENSO Transition. Science 291, 2594–2597. https://doi.org/10.1126/science.1055071

Bent, S.M., Muratore, D., Becker, K.W., Barone, B., Clemente, T., Fredricks, H.F., Holm, H.C., Karl, D.M., Van Mooy, B.A.S., 2024. Lipid biochemical diversity and dynamics reveal phytoplankton nutrient-stress responses and carbon export mechanisms in mesoscale eddies in the North Pacific Subtropical Gyre. Frontiers in Marine Science 11, 1427524. https://doi.org/10.3389/fmars.2024.1427524

Bidle, K.D., Azam, F., 1999. Accelerated dissolution of diatom silica by marine bacterial assemblages. Nature 397, 508–512. https://doi.org/10.1038/17351

Bodel, A., Estapa, M., Durkin, C.A., 2025. Solitary phytoplankton cells sink in the mesopelagic ocean. PLOS ONE 20, e0321918. https://doi.org/10.1371/journal.pone.0321918

Boyd, P.W., Claustre, H., Levy, M., Siegel, D.A., Weber, T., 2019. Multi-faceted particle pumps drive carbon sequestration in the ocean. Nature 568, 327–335. https://doi.org/10.1038/s41586-019-1098-2

Boyd, P.W., Stevens, C.L., 2002. Modelling particle transformations and the downward organic carbon flux in the NE Atlantic Ocean. Progress in Oceanography 52, 1–29. https://doi.org/10.1016/S0079-6611(02)00020-4

Briggs, N., Dall'Olmo, G., Claustre, H., 2020. Major role of particle fragmentation in regulating biological sequestration of CO_2 by the oceans. Science 367, 791–793. https://doi.org/10.1126/science.aay1790

Cantarero, S.I., Flores, E., Allbrook, H., Aguayo, P., Vargas, C.A., Tamanaha, J.E., Scholz, J.B.C., Bach, L.T., Löscher, C.R., Riebesell, U., Rajagopalan, B., Dildar, N., Sepúlveda, J., 2024. Lipid remodeling in phytoplankton exposed to multi-environmental drivers in a

mesocosm experiment. Biogeosciences 21, 3927–3958. https://doi.org/10.5194/bg-21-3927-2024

Collins, J.R., Edwards, B.R., Thamatrakoln, K., Ossolinski, J.E., DiTullio, G.R., Bidle, K.D., Doney, S.C., Van Mooy, B.A.S., 2015. The multiple fates of sinking particles in the North Atlantic Ocean. Global Biogeochemical Cycles 29, 1471–1494. https://doi.org/10.1002/2014GB005037

Dauwe, B., Middelburg, J.J., Herman, P.M.J., Heip, C.H.R., 1999. Linking diagenetic alteration of amino acids and bulk organic matter reactivity. Limnology and Oceanography 44, 1809–1814. https://doi.org/10.4319/lo.1999.44.7.1809

DeVries, T., 2022. The Ocean Carbon Cycle. Annual Review of Environment and Resources 47, 317–341. https://doi.org/10.1146/annurev-environ-120920-111307

DeVries, T., Weber, T., 2017. The export and fate of organic matter in the ocean: New constraints from combining satellite and oceanographic tracer observations. Global Biogeochemical Cycles 31, 535–555. https://doi.org/10.1002/2016GB005551

Doherty, S.C., Maas, A.E., Steinberg, D.K., Popp, B.N., Close, H.G., 2021. Distinguishing zooplankton fecal pellets as a component of the biological pump using compound-specific isotope analysis of amino acids. Limnology and Oceanography 66, 2827–2841. https://doi.org/10.1002/lno.11793

Durkin, C.A., Buesseler, K.O., Cetinić, I., Estapa, M.L., Kelly, R.P., Omand, M., 2021. A Visual Tour of Carbon Export by Sinking Particles. Global Biogeochemical Cycles 35, e2021GB006985. https://doi.org/10.1029/2021GB006985

Estapa, M., Buesseler, K., Durkin, C.A., Omand, M., Benitez-Nelson, C.R., Roca-Martí, M., Breves, E., Kelly, R.P., Pike, S., 2021. Biogenic sinking particle fluxes and sediment trap

collection efficiency at Ocean Station Papa. Elementa: Science of the Anthropocene 9, 00122. https://doi.org/10.1525/elementa.2020.00122

Estapa, M., Valdes, J., Tradd, K., Sugar, J., Omand, M., Buesseler, K., 2020. The Neutrally Buoyant Sediment Trap: Two Decades of Progress. Journal of Atmospheric and Oceanic Technology 37, 957–973. https://doi.org/10.1175/JTECH-D-19-0118.1

Fulton, J.M., Fredricks, H.F., Van Mooy, B.A.S., 2017. Intact polar lipid export in the temperate western North Atlantic and Sargasso Sea. Organic Geochemistry 114, 45–56. https://doi.org/10.1016/j.orggeochem.2017.09.005

Gašparović, B., Penezić, A., Lampitt, R.S., Sudasinghe, N., Schaub, T., 2016. Free fatty acids, tri-, di- and monoacylglycerol production and depth-related cycling in the Northeast Atlantic. Marine Chemistry 186, 101–109. https://doi.org/10.1016/j.marchem.2016.09.002

Goddard-Borger, E.D., Williams, S.J., 2017. Sulfoquinovose in the biosphere: occurrence, metabolism and functions. Biochemical Journal 474, 827–849. https://doi.org/10.1042/BCJ20160508

Goutx, M., Guigue, C., Striby, L., 2003. Triacylglycerol biodegradation experiment in marine environmental conditions: definition of a new lipolysis index. Organic Geochemistry 34, 1465–1473. https://doi.org/10.1016/S0146-6380(03)00119-0

Goutx, M., Momzikoff, A., Striby, L., Andersen, V., Marty, J.C., Vescovali, I., 2000. High-frequency fluxes of labile compounds in the central Ligurian Sea, northwestern Mediterranean. Deep Sea Research Part I: Oceanographic Research Papers 47, 533–556. https://doi.org/10.1016/S0967-0637(99)00101-6

795 Goutx, M., Wakeham, S.G., Lee, C., Duflos, M., Guigue, C., Liu, Z., Moriceau, B., Sempére, R.,
796 Tedetti, M., Xue, J., 2007. Composition and degradation of marine particles with different
797 settling velocities in the northwestern Mediterranean Sea. Limnology and Oceanography
798 52, 1645–1664. https://doi.org/10.4319/lo.2007.52.4.1645
799 Harvey, H., Fallon, R., Patton, J., 1986. The effect of organic matter and oxygen on the
800 degradation of bacterial membrane lipids in marine sediments. Geochimica et
801 Cosmochimica Acta 50, 795–804. https://doi.org/10.1016/0016-7037(86)90355-8
802 Hedges, J.I., Baldock, J.A., Gélinas, Y., Lee, C., Peterson, M., Wakeham, S.G., 2001. Evidence
803 for non-selective preservation of organic matter in sinking marine particles. Nature 409,
804 801–804. https://doi.org/10.1038/35057247
805 Holm, H.C., Fredricks, H.F., Bent, S.M., Lowenstein, D.P., Ossolinski, J.E., Becker, K.W.,
806 Johnson, W.M., Schrage, K., Mooy, B.A.S.V., 2022. Global ocean lipidomes show a
807 universal relationship between temperature and lipid unsaturation. Science 376, 1487–
808 1491. https://doi.org/10.1126/science.abn7455
809 Holm, H.C., Fredricks, H.F., Bent, S.M., Lowenstein, D.P., Schrage, K.R., Van Mooy, B.A.S.,
810 2024. Lipid composition, caloric content, and novel oxidation products from microbial
811 communities within seasonal pack ice cores. Geochimica et Cosmochimica Acta 368, 12–
812 23. https://doi.org/10.1016/j.gca.2024.01.003
813 Hunter, J.E., Fredricks, H.F., Behrendt, L., Alcolombri, U., Bent, S.M., Stocker, R., Van Mooy,
814 B.A.S., 2021. Using High-Sensitivity Lipidomics To Assess Microscale Heterogeneity in
815 Oceanic Sinking Particles and Single Phytoplankton Cells. Environmental Science &
816 Technology 55, 15456–15465. https://doi.org/10.1021/acs.est.1c02836

Isles, P.D.F., 2020. The misuse of ratios in ecological stoichiometry. Ecology 101. https://doi.org/10.1002/ecy.3153

Iversen, M.H., 2023. Carbon Export in the Ocean: A Biologist's Perspective. Annual Review of Marine Science 15, 357–381. https://doi.org/10.1146/annurev-marine-032122-035153

Johnson, L., Siegel, D.A., Thompson, A.F., Fields, E., Erickson, Z.K., Cetinic, I., Lee, C.M., D'Asaro, E.A., Nelson, N.B., Omand, M.M., Sten, M., Traylor, S., Nicholson, D.P., Graff, J.R., Steinberg, D.K., Sosik, H.M., Buesseler, K.O., Brzezinski, M.A., Ramos, I.S., Carvalho, F., Henson, S.A., 2024. Assessment of oceanographic conditions during the North Atlantic EXport processes in the ocean from RemoTe sensing (EXPORTS) field campaign. Progress in Oceanography 220, 103170. https://doi.org/10.1016/j.pocean.2023.103170

Johnson, W.M., Longnecker, K., Kido Soule, M.C., Arnold, W.A., Bhatia, M.P., Hallam, S.J., Van Mooy, B.A.S., Kujawinski, E.B., 2020. Metabolite composition of sinking particles differs from surface suspended particles across a latitudinal transect in the South Atlantic. Limnology and Oceanography 65, 111–127. https://doi.org/10.1002/lno.11255

Krupke, A., Hmelo, L.R., Ossolinski, J.E., Mincer, T.J., Van Mooy, B.A.S., 2016. Quorum Sensing Plays a Complex Role in Regulating the Enzyme Hydrolysis Activity of Microbes Associated with Sinking Particles in the Ocean. Frontiers in Marine Science 3. https://doi.org/10.3389/fmars.2016.00055

Laurenceau-Cornec, E.C., Trull, T.W., Davies, D.M., Bray, S.G., Doran, J., Planchon, F., Carlotti, F., Jouandet, M.-P., Cavagna, A.-J., Waite, A.M., Blain, S., 2015. The relative importance of phytoplankton aggregates and zooplankton fecal pellets to carbon export: insights from free-drifting sediment trap deployments in naturally iron-fertilised waters near the

Kerguelen Plateau. Biogeosciences 12, 1007–1027. https://doi.org/10.5194/bg-12-1007-2015

Lee, C., Wakeham, S., Arnosti, C., 2004. Particulate organic matter in the sea: the composition conundrum. Ambio 33, 565–575. https://doi.org/10.1579/0044-7447-33.8.565

Martin, J.H., Knauer, G.A., Karl, D.M., Broenkow, W.W., 1987. VERTEX: carbon cycling in the northeast Pacific. Deep Sea Research Part A. Oceanographic Research Papers 34, 267–285. https://doi.org/10.1016/0198-0149(87)90086-0

McNair, H.M., Meyer, M.G., Lerch, S.J., Maas, A.E., Stephens, B.M., Fox, J., Buck, K.N., Burns, S.M., Cetinić, I., Cohn, M., Durkin, C., Gifford, S., Gong, W., Graff, J.R., Jenkins, B., Jones, E.L., Santoro, A.E., Shea, C.H., Stamieszkin, K., Steinberg, D.K., Marchetti, A., Carlson, C.A., Menden-Deuer, S., Brzezinski, M.A., Siegel, D.A., Rynearson, T.A., 2023. Quantitative analysis of food web dynamics in a low export ecosystem. https://doi.org/10.1101/2023.03.17.532807

Meyer, M.G., Brzezinski, M.A., Cohn, M.R., Kramer, S.J., Paul, N., Sharpe, G., Niebergall, A.K., Gifford, S., Cassar, N., Marchetti, A., 2023. Primary production dynamics during the decline phase of the North Atlantic annual spring bloom. https://doi.org/10.1101/2023.05.18.541304

Meyer, M.G., Gong, W., Kafrissen, S.M., Torano, O., Varela, D.E., Santoro, A.E., Cassar, N., Gifford, S., Niebergall, A.K., Sharpe, G., Marchetti, A., 2022. Phytoplankton size-class contributions to new and regenerated production during the EXPORTS Northeast Pacific Ocean field deployment. Elementa: Science of the Anthropocene 10, 00068. https://doi.org/10.1525/elementa.2021.00068

862 Moodley, L., Boschker, H.T.S., Middelburg, J.J., Pel, R., Herman, P.M.J., Deckere, E. de, Heip,
863 C.H.R., 2000. Ecological significance of benthic foraminifera: 13C labelling
864 experiments. Marine Ecology Progress Series 202, 289–295.
865 https://doi.org/10.3354/meps202289
866 Nowicki, M., DeVries, T., Siegel, D.A., 2022. Quantifying the Carbon Export and Sequestration
867 Pathways of the Ocean's Biological Carbon Pump. Global Biogeochemical Cycles 36,
868 e2021GB007083. https://doi.org/10.1029/2021GB007083
869 Omand, M.M., Govindarajan, R., He, J., Mahadevan, A., 2020. Sinking flux of particulate
870 organic matter in the oceans: Sensitivity to particle characteristics. Scientific Reports 10,
871 5582. https://doi.org/10.1038/s41598-020-60424-5
872 Pantoja, S., Rossel, P., Castro, R., Cuevas, L.A., Daneri, G., Córdova, C., 2009. Microbial
873 degradation rates of small peptides and amino acids in the oxygen minimum zone of
874 Chilean coastal waters. Deep Sea Research Part II: Topical Studies in Oceanography, The
875 Oceanography of the Eastern South Pacific II: The Oxygen Minimum Zone 56, 1055–
876 1062. https://doi.org/10.1016/j.dsr2.2008.09.007
877 Passow, U., 2002. Transparent exopolymer particles (TEP) in aquatic environments. Progress in
878 Oceanography 55, 287–333. https://doi.org/10.1016/S0079-6611(02)00138-6
879 Popendorf, K.J., Lomas, M.W., Van Mooy, B.A.S., 2011. Microbial sources of intact polar
880 diacylglycerolipids in the Western North Atlantic Ocean. Organic Geochemistry 42, 803–
881 811. https://doi.org/10.1016/j.orggeochem.2011.05.003
882 Roca-Martí, M., Benitez-Nelson, C.R., Umhau, B.P., Wyatt, A.M., Clevenger, S.J., Pike, S.,
883 Horner, T.J., Estapa, M.L., Resplandy, L., Buesseler, K.O., 2021. Concentrations, ratios,

884 and sinking fluxes of major bioelements at Ocean Station Papa. Elementa: Science of the
885 Anthropocene 9, 00166. https://doi.org/10.1525/elementa.2020.00166
886 Sarmiento, J.L., Gruber, N., 2006. Ocean biogeochemical dynamics. Princeton University Press,
887 Princeton.
888 Schouten, S., Middelburg, J.J., Hopmans, E.C., Sinninghe Damsté, J.S., 2010. Fossilization and
889 degradation of intact polar lipids in deep subsurface sediments: A theoretical approach.
890 Geochimica et Cosmochimica Acta 74, 3806–3814.
891 https://doi.org/10.1016/j.gca.2010.03.029
892 Shea, C.H., Wojtal, P.K., Close, H.G., Maas, A.E., Stamieszkin, K., Cope, J.S., Steinberg, D.K.,
893 Wallsgrove, N., Popp, B.N., 2023. Small particles and heterotrophic protists support the
894 mesopelagic zooplankton food web in the subarctic northeast Pacific Ocean. Limnology
895 and Oceanography n/a. https://doi.org/10.1002/lno.12397
896 Sheridan, C.C., Lee, C., Wakeham, S.G., Bishop, J.K.B., 2002. Suspended particle organic
897 composition and cycling in surface and midwaters of the equatorial Pacific Ocean. Deep
898 Sea Research Part I: Oceanographic Research Papers 49, 1983–2008.
899 https://doi.org/10.1016/S0967-0637(02)00118-8
900 Siegel, D.A., Cetinić, I., Graff, J.R., Lee, C.M., Nelson, N., Perry, M.J., Ramos, I.S., Steinberg,
901 D.K., Buesseler, K., Hamme, R., Fassbender, A.J., Nicholson, D., Omand, M.M., Robert,
902 M., Thompson, A., Amaral, V., Behrenfeld, M., Benitez-Nelson, C., Bisson, K., Boss, E.,
903 Boyd, P.W., Brzezinski, M., Buck, K., Burd, A., Burns, S., Caprara, S., Carlson, C.,
904 Cassar, N., Close, H., D'Asaro, E., Durkin, C., Erickson, Z., Estapa, M.L., Fields, E.,
905 Fox, J., Freeman, S., Gifford, S., Gong, W., Gray, D., Guidi, L., Haëntjens, N., Halsey,
906 K., Huot, Y., Hansell, D., Jenkins, B., Karp-Boss, L., Kramer, S., Lam, P., Lee, J.-M.,

907 Maas, A., Marchal, O., Marchetti, A., McDonnell, A., McNair, H., Menden-Deuer, S.,
908 Morison, F., Niebergall, A.K., Passow, U., Popp, B., Potvin, G., Resplandy, L., Roca-
909 Martí, M., Roesler, C., Rynearson, T., Traylor, S., Santoro, A., Seraphin, K.D., Sosik,
910 H.M., Stamieszkin, K., Stephens, B., Tang, W., Van Mooy, B., Xiong, Y., Zhang, X.,
911 2021. An operational overview of the EXport Processes in the Ocean from RemoTe
912 Sensing (EXPORTS) Northeast Pacific field deployment. Elementa: Science of the
913 Anthropocene 9, 00107. https://doi.org/10.1525/elementa.2020.00107
914 Siegel, D.A., DeVries, T., Cetinić, I., Bisson, K.M., 2023. Quantifying the Ocean's Biological
915 Pump and Its Carbon Cycle Impacts on Global Scales. Annual Review of Marine Science
916 15, 329–356. https://doi.org/10.1146/annurev-marine-040722-115226
917 Smith, D.C., Simon, M., Alldredge, A.L., Azam, F., 1992. Intense hydrolytic enzyme activity on
918 marine aggregates and implications for rapid particle dissolution. Nature 359, 139–142.
919 https://doi.org/10.1038/359139a0
920 Turner, J.T., 2015. Zooplankton fecal pellets, marine snow, phytodetritus and the ocean's
921 biological pump. Progress in Oceanography 130, 205–248.
922 https://doi.org/10.1016/j.pocean.2014.08.005
923 Ucar, I., Pebesma, E., Azcorra, A., 2018. Measurement Errors in R. The R Journal 10, 549–557.
924 https://doi.org/10.32614/RJ-2018-075
925 Van Mooy, B.A.S., Fredricks, H.F., 2010. Bacterial and eukaryotic intact polar lipids in the
926 eastern subtropical South Pacific: Water-column distribution, planktonic sources, and
927 fatty acid composition. Geochimica et Cosmochimica Acta 74, 6499–6516.
928 https://doi.org/10.1016/j.gca.2010.08.026

Van Mooy, B.A.S., Keil, R.G., Devol, A.H., 2002. Impact of suboxia on sinking particulate organic carbon: Enhanced carbon flux and preferential degradation of amino acids via denitrification. Geochimica et Cosmochimica Acta 66, 457–465. https://doi.org/10.1016/S0016-7037(01)00787-6

Wakeham, S.G., Canuel, E.A., 1988. Organic geochemistry of particulate matter in the eastern tropical North Pacific Ocean: Implications for particle dynamics. Journal of Marine Research 46, 183–213. https://doi.org/10.1357/002224088785113748

Wakeham, S.G., Lee, C., Hedges, J.I., Hernes, P.J., Peterson, M.J., 1997. Molecular indicators of diagenetic status in marine organic matter. Geochimica et Cosmochimica Acta 61, 5363–5369. https://doi.org/https://doi.org/10.1016/S0016-7037(97)00312-8

Westberry, T., Behrenfeld, M.J., Siegel, D.A., Boss, E., 2008. Carbon-based primary productivity modeling with vertically resolved photoacclimation. Global Biogeochemical Cycles 22. https://doi.org/10.1029/2007GB003078

Wojtal, P.K., Doherty, S.C., Shea, C.H., Popp, B.N., Benitez-Nelson, C.R., Buesseler, K.O., Estapa, M.L., Roca-Martí, M., Close, H.G., 2023. Deconvolving mechanisms of particle flux attenuation using nitrogen isotope analyses of amino acids. Limnology and Oceanography n/a. https://doi.org/10.1002/lno.12398

Xue, J., Lee, C., Wakeham, S.G., Armstrong, R.A., 2011. Using principal components analysis (PCA) with cluster analysis to study the organic geochemistry of sinking particles in the ocean. Organic Geochemistry 42, 356–367. https://doi.org/10.1016/j.orggeochem.2011.01.012

Figure Captions:

Figure 1. Flux profiles of major glycerolipid classes from North Pacific and North Atlantic sites. Fluxes are shown for TGs (A), DGs (B), MGs (C), and all nine classes of IPLs combined (D). The combined flux of all glycerolipids is shown in panel (E). The total POC flux is shown in panel (F). Correlation between the total glycerolipid flux and total POC flux is shown in panel (G). Annotation shows the slope of the line of best fit as well as lines corresponding to a 1% and 5% slope. Coefficient of determination (R^2) and significance level (p) for linear fit are shown in the top left. The trap type (NBST or STT) is designated with point shape. Color corresponds to the location (North Pacific or North Atlantic) and sampling period when traps were deployed. Lines are drawn in profiles connecting samples from the same sampling period and trap type. Panel (H) shows globe with approximate location of sample collection.

Figure 2. Compositional bar plots of sinking glycerolipid flux. Panels A-C show the percent of glycerolipid carbon TGs, DGs, MGs, and IPLs contribute to total glycerolipid carbon flux (x-axis) with increasing sample collection depth (y-axis). Panels D-F breaks IPLs down further based on headgroup and shows the percentage each IPL class contributes to total IPL carbon flux (x-axis) with increasing depth (y-axis). Panels correspond to separate deployment periods: North Pacific (A and D), early North Atlantic (B and E), and late North Atlantic (C and F). Color indicates lipid class.

Figure 3. nMDS ordination plots for sinking and suspended lipid samples. Panel A shows nMDS ordination for just the sinking samples from both sites. Panel B shows nMDS ordination for sinking and suspended material combined from both sites. Arrows show tested metadata vectors for gradients across samples. Arrow length shows correlation strength and direction of gradient. Significant vectors ($p < 0.05$) are noted with an asterisk. The collection type (NBTS or

975 STT for sinking, CTD for suspended) is designated with point shape. Color corresponds to the
976 location (North Pacific or north Atlantic) and sampling period for sinking material. Suspended
977 material shown was collected through the full duration of both campaigns.

978 **Figure 4. Mean unsaturation of SQDG versus depth in sinking and suspended material.**
979 Panels show suspended and sinking material from North Pacific (A) and North Atlantic (B) sites
980 respectively. The x-axis corresponds to the mean unsaturation per fatty acid for SQDG molecules
981 in each sample. The y-axis shows sample depth. Red lines correspond to the predicted mean
982 unsaturation based on water temperature at time of suspend material collection using fit from Holm
983 *et al.* 2022. Grey region indicate the 95% prediction intervals of temperature-based unsaturation
984 predictions. This trendline has been smoothed with loess smoothing (α = 0.75). Individual
985 suspended material samples collected from CTD or ship flowthrough system are shown in grey.
986 Dashed line show approximate bottom of photic zone (1% of surface photosynthetically active
987 radiation). Point colors for sinking material correspond to the location and sampling period.
988 Suspended material shown here was collected through the full duration of both campaigns.

989 **Figure 5. Glycerolipid source and degradation indices in sinking material.** Particle source
990 (LD_{LIP}, A) and lipid hydrolysis (LI_{MOD}, B) indices are shown versus depth for all three sampling
991 periods. Panel C shows the correlation between LD_{LIP} and the log10 ratio of aggregates to fecal
992 pellets as assessed by optical gel imaging. Panel D shows the correlation between the LI_{MOD} and
993 LD_{LIP} indices. Panel E shows the correlation between LI_{MOD} and the log10 ratio of aggregates to
994 fecal pellets as assessed by optical gel imaging. Coefficient of determination (R^2) and significance
995 level (p) for linear fit are shown in panel of C, D, and E. In panels C and E, the linear correlation
996 is shown for all points (solid line, unstarred coefficients) and with one stared outlier sample
997 removed (dashed line, starred coefficients). The trap type (NBTS or STT) is designated with point

shape. Color corresponds to the location and sampling period when traps were deployed. Lines are drawn in profiles connecting samples from the same sampling period and trap type. Error bars for lipid indices represent a best estimate of analytical error (see Methods section 2.6 and 2.7).

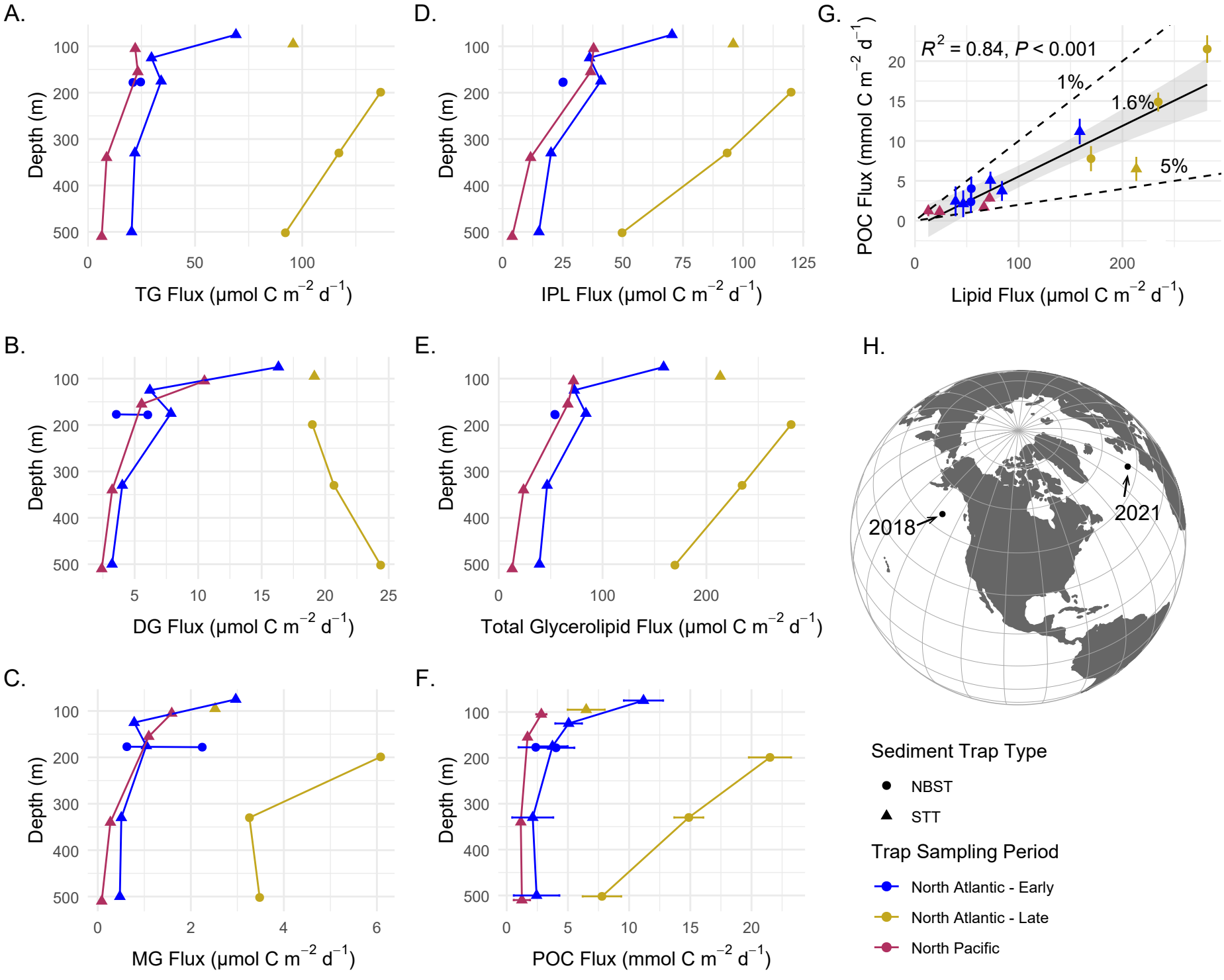
A.
B.
C.
D.
E.
F.
G.
H.
Depth (m)
TG Flux (μmol C m^{-2} d^{-1})
DG Flux (μmol C m^{-2} d^{-1})
MG Flux (μmol C m^{-2} d^{-1})
IPL Flux (μmol C m^{-2} d^{-1})
Total Glycerolipid Flux (μmol C m^{-2} d^{-1})
POC Flux (mmol C m^{-2} d^{-1})
R^2 = 0.84, P < 0.001
1%
1.6%
5%
Lipid Flux (μmol C m^{-2} d^{-1})
2018
2021
Sediment Trap Type
NBST
STT
Trap Sampling Period
North Atlantic - Early
North Atlantic - Late
North Pacific

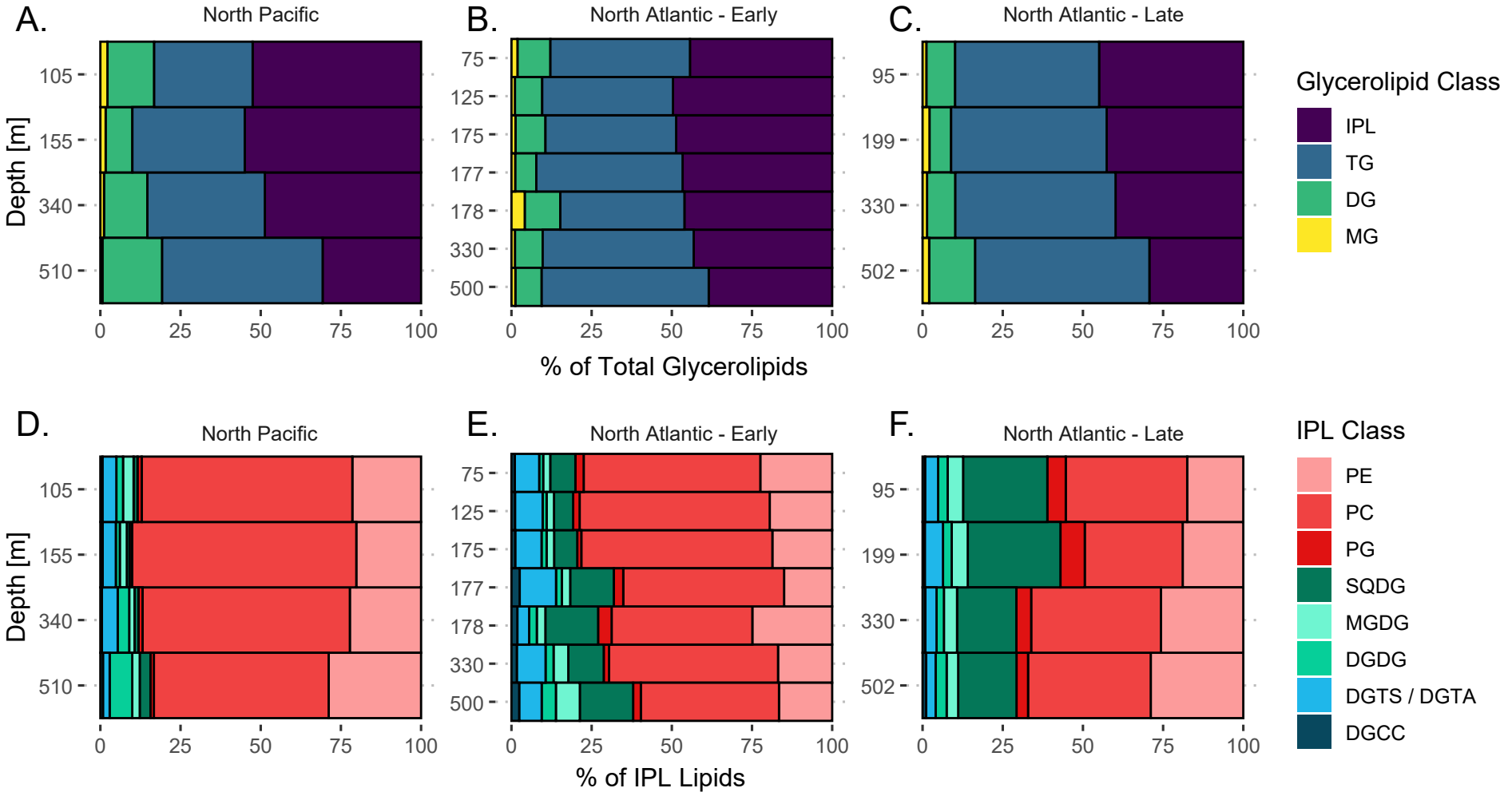
A.
North Pacific
B.
North Atlantic - Early
C.
North Atlantic - Late
Depth [m]
105
155
340
510
75
125
175
177
178
330
500
95
199
330
502
0
25
50
75
100
% of Total Glycerolipids
Glycerolipid Class
IPL
TG
DG
MG
D.
North Pacific
E.
North Atlantic - Early
F.
North Atlantic - Late
% of IPL Lipids
IPL Class
PE
PC
PG
SQDG
MGDG
DGDG
DGTS / DGTA
DGCC

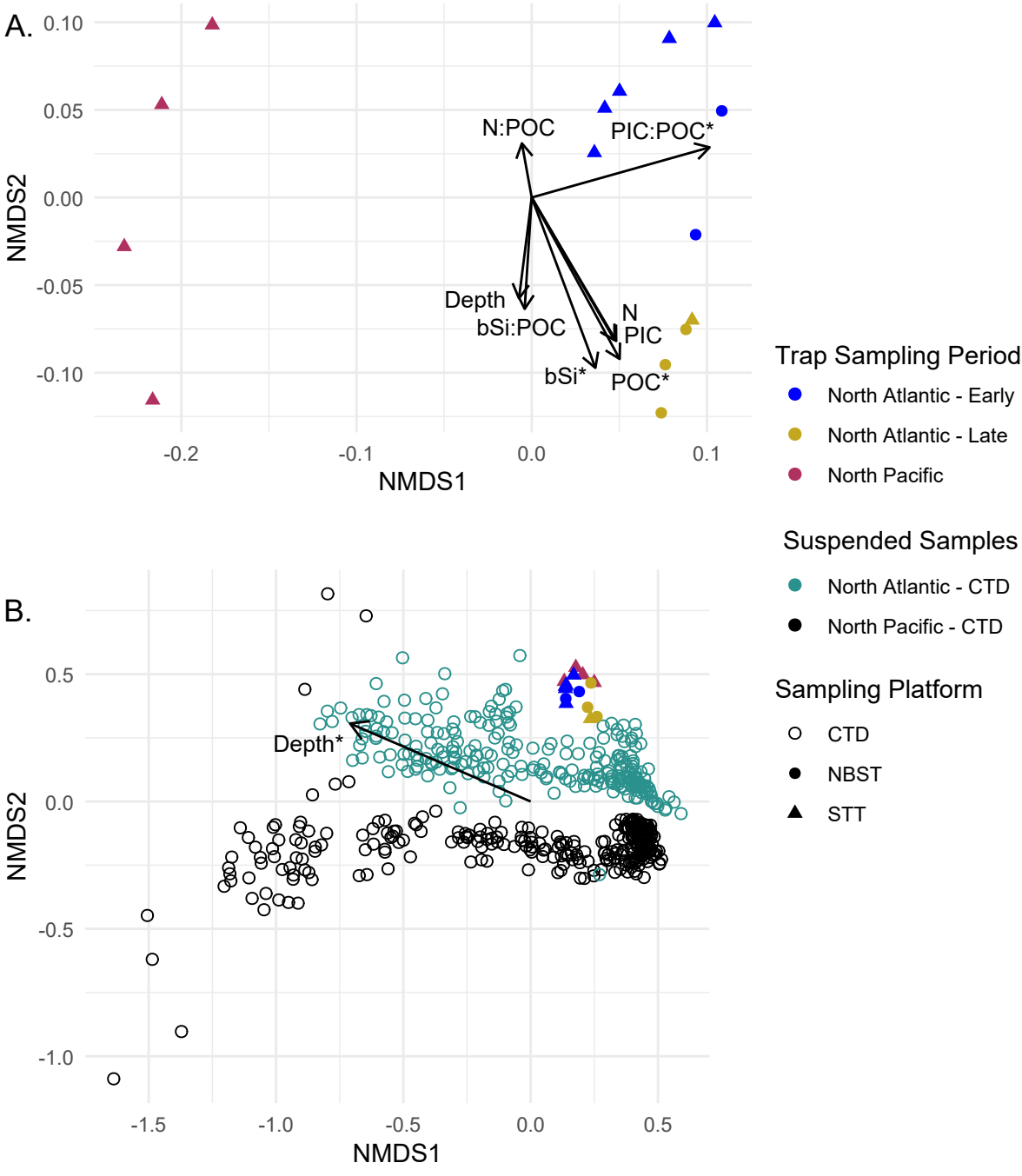
A.
0.10
0.05
0.00
-0.05
-0.10
NMDS2
-0.2
-0.1
0.0
0.1
NMDS1
N:POC
PIC:POC*
Depth
bSi:POC
N
PIC
bSi*
POC*
B.
0.5
0.0
-0.5
-1.0
NMDS2
-1.5
-1.0
-0.5
0.0
0.5
NMDS1
Depth*
Trap Sampling Period
North Atlantic - Early
North Atlantic - Late
North Pacific
Suspended Samples
North Atlantic - CTD
North Pacific - CTD
Sampling Platform
CTD
NBST
STT

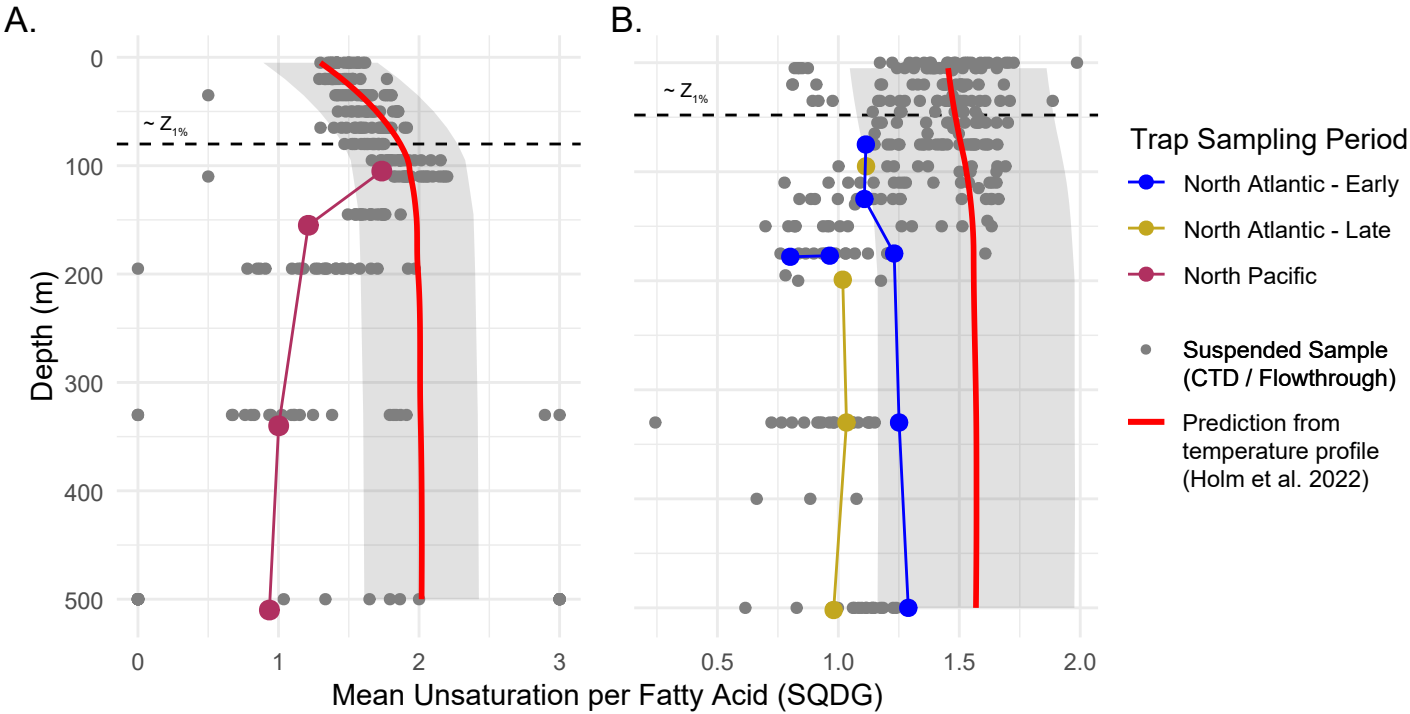
A.
B.
~ Z1%
~ Z1%
Depth (m)
0
100
200
300
400
500
0
1
2
3
0.5
1.0
1.5
2.0
Mean Unsaturation per Fatty Acid (SQDG)
Trap Sampling Period
North Atlantic - Early
North Atlantic - Late
North Pacific
Suspended Sample (CTD / Flowthrough)
Prediction from temperature profile (Holm et al. 2022)

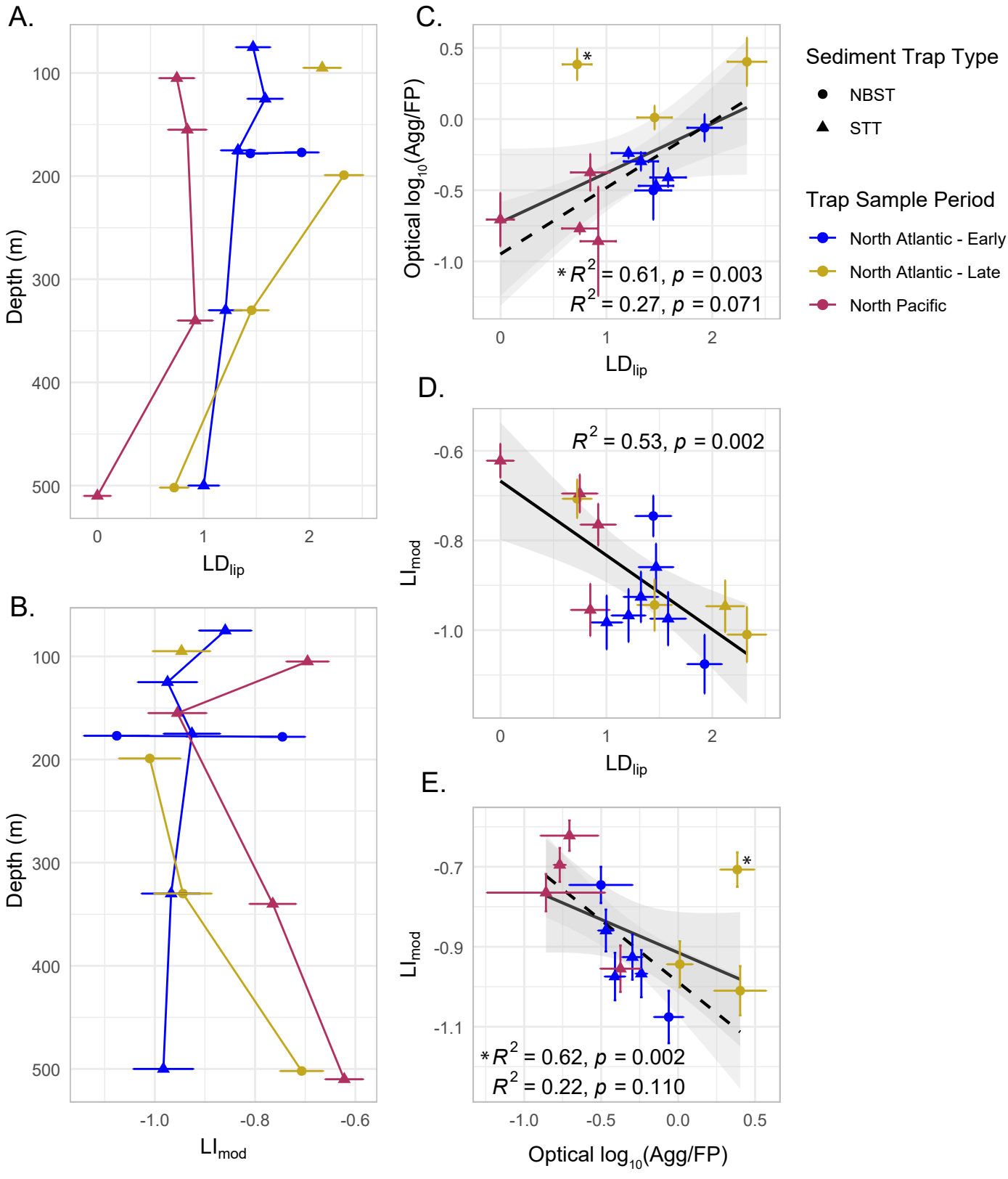
A.
B.
C.
D.
E.
Depth (m)
100
200
300
400
500
0
1
2
LDlip
-1.0
-0.8
-0.6
LImod
Optical log10(Agg/FP)
0.5
0.0
-0.5
-1.0
*R2 = 0.61, p = 0.003
R2 = 0.27, p = 0.071
R2 = 0.53, p = 0.002
-0.7
-0.9
-1.1
*R2 = 0.62, p = 0.002
R2 = 0.22, p = 0.110
Sediment Trap Type
NBST
STT
Trap Sample Period
North Atlantic - Early
North Atlantic - Late
North Pacific

Supplementary Material for

Glycerolipids track sinking particle sources and remineralization in two ocean basins

Henry C. Holm[a,b*], Helen F. Fredricks[a], and Benjamin A. S. Van Mooy[a]

Affiliations:

[a]Marine Chemistry and Geochemistry Department, Woods Hole Oceanographic Institution; Woods Hole, MA 02543, USA

[b]MIT-WHOI Joint Program in Oceanography/Applied Ocean Science & Engineering; Cambridge, MA, 02139, USA

*Corresponding author. Email: hholm@ldeo.columbia.edu

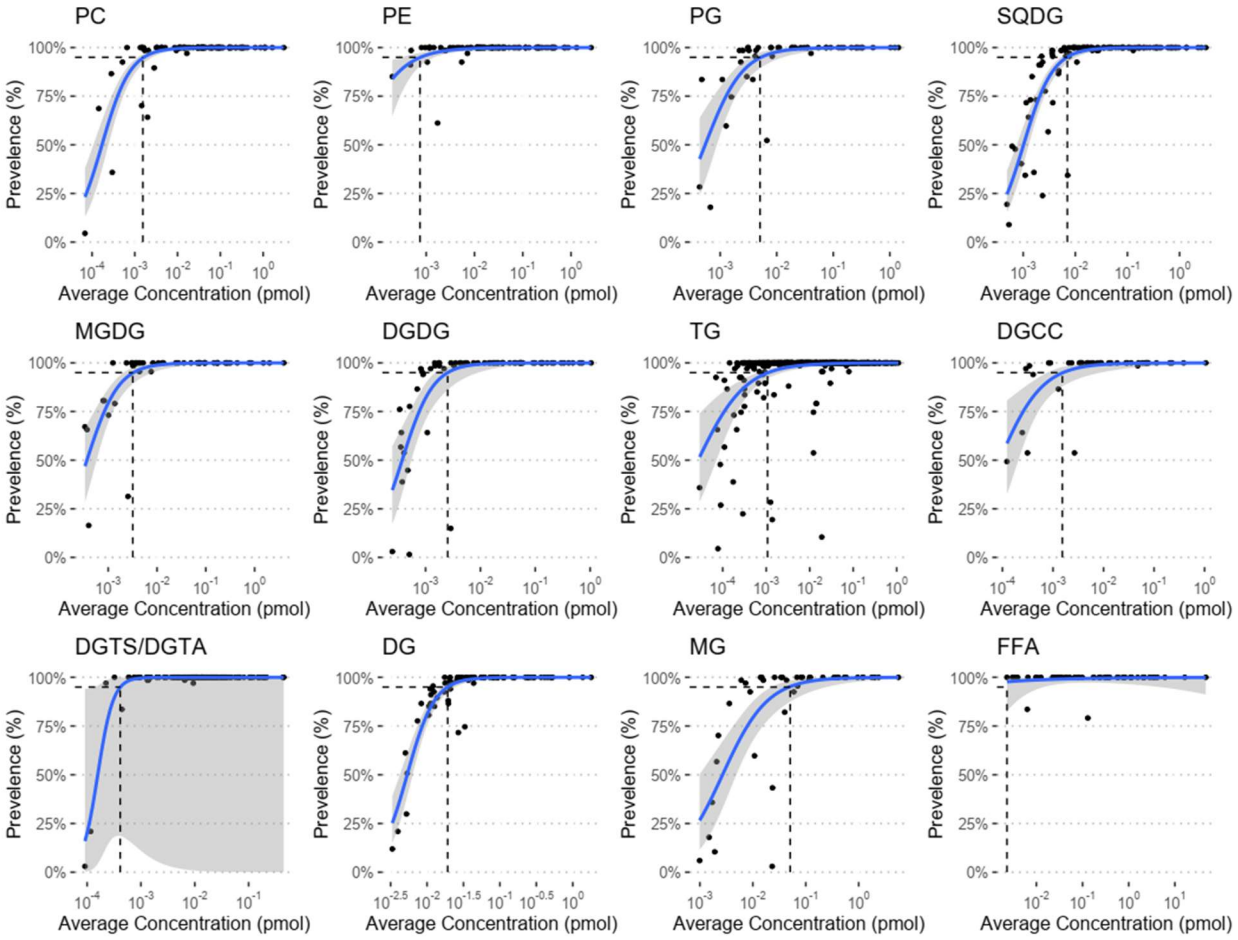

Supplementary Figure 1. Calculation of LOD for each lipid class via repeated QC measurements. Each panel shows the prevalence of lipid species in repeat QC samples (y-axis) versus the concentration of said species when it was detectable (x-axis). The blue line shows a quasibinomial fit to the data. The dashed lines show the modeled concentration at which species from a given class were no longer detectable 95% of the time.

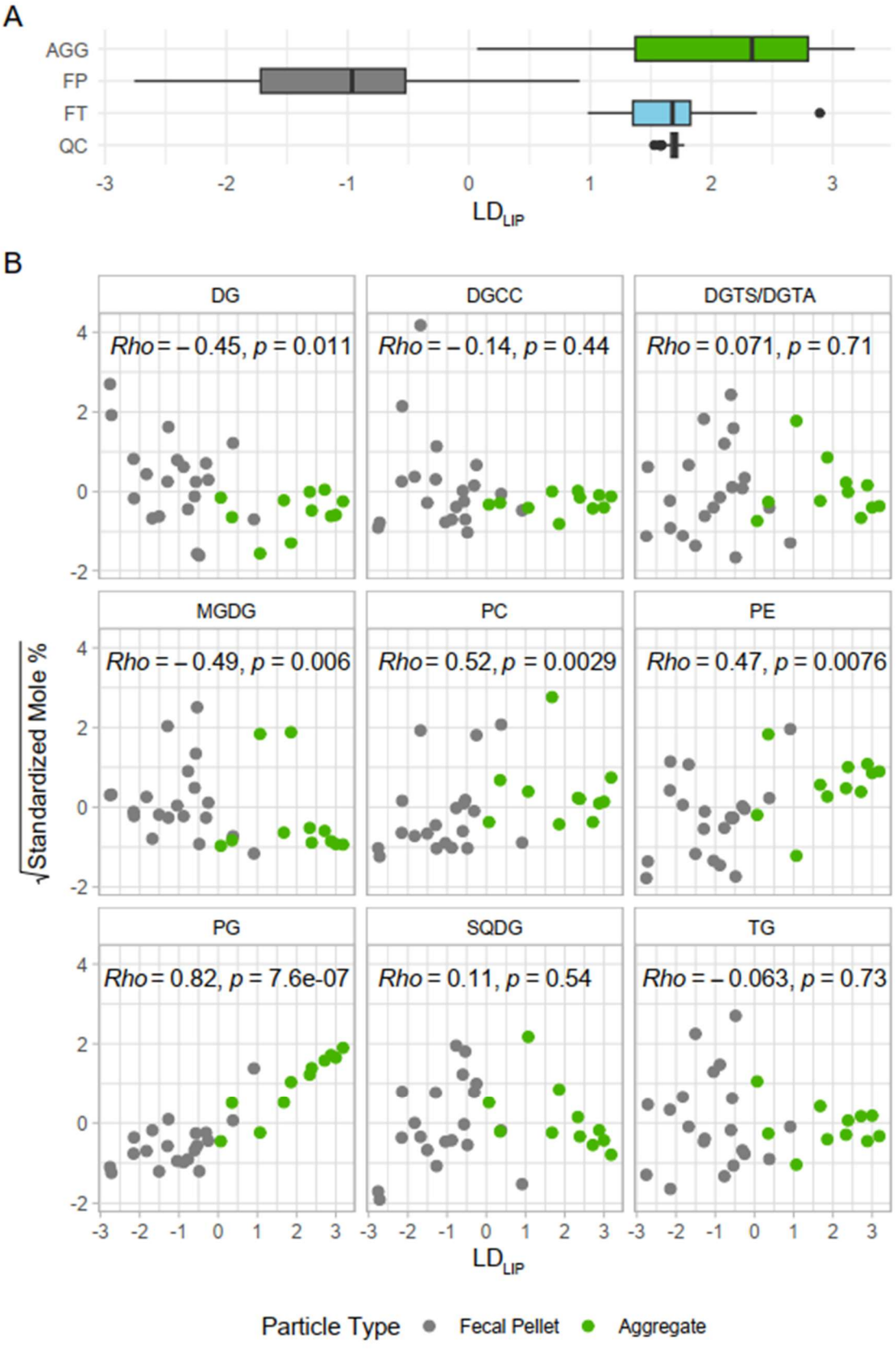
A
AGG
FP
FT
QC
-3
-2
-1
0
1
2
3
LD_LIP
B
DG
Rho = – 0.45, p = 0.011
DGCC
Rho = – 0.14, p = 0.44
DGTS/DGTA
Rho = 0.071, p = 0.71
MGDG
Rho = – 0.49, p = 0.006
PC
Rho = 0.52, p = 0.0029
PE
Rho = 0.47, p = 0.0076
PG
Rho = 0.82, p = 7.6e-07
SQDG
Rho = 0.11, p = 0.54
TG
Rho = – 0.063, p = 0.73
√Standardized Mole %
4
2
0
-2
LD_LIP
Particle Type
Fecal Pellet
Aggregate

Supplementary Figure 2. **LD_{LIP} results for single particle training data**. Panel (A) shows the LD_{LIP} index (x-axis) for single particle training data aggregates (AGG, n = 20) and fecal pellets (FP, n = 11). The index is also shown for suspended surface material collected on the flowthrough system in the North Atlantic (FT, n = 23) as well as identical quality control samples of pooled EXPORTS lipid extracts to assess analytical variability in the index (QC, n = 67). Panel (B) shows the relationship between lipid training data and final LD_{LIP} metric. Spearman rank (Rho) coefficient and p-value for relationship are shown in each panel.

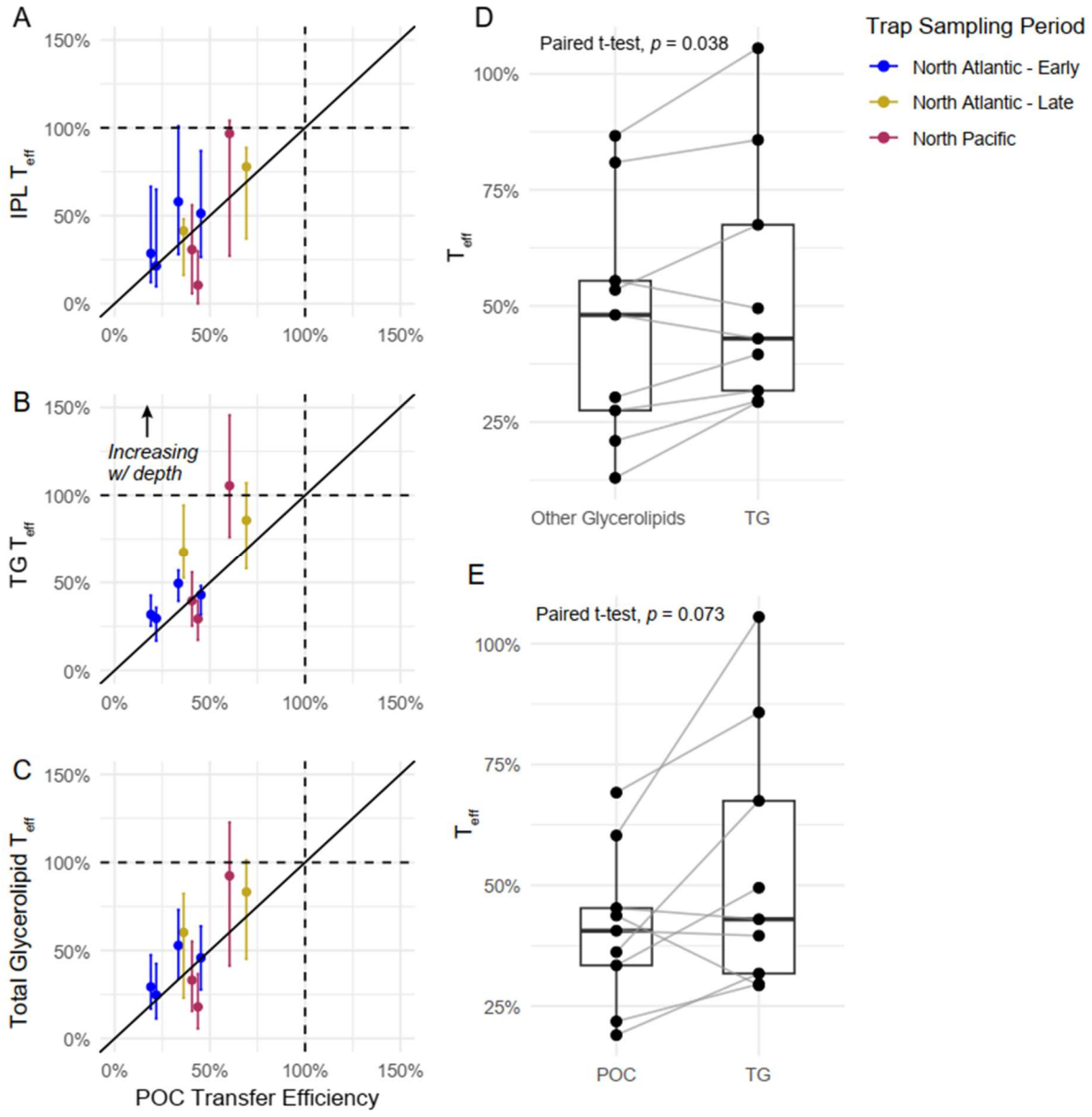

Supplementary Figure 3. **Transfer efficiency (T_{eff}) of glycerolipids classes verse POC across multiple depth horizons.** T_{eff} of lipid mass and POC were calculated from the surface most trap of each sampling period to multiple depth horizons. Panel (A) shows the T_{eff} of all IPLs verse POC. Panel (B) shows the T_{eff} of all TGs verse POC. Panel (C) shows the T_{eff} of all glycerolipids verse POC. Points represent the T_{eff} of all summed lipid mass. Error bars indicate the 25th and 75th percentile T_{eff} for individual lipid species within summed group. T_{eff} greater than 100% indicates increasing flux with depth. Panel (D) shows results of paired t-test between T_{eff} of TGs and T_{eff} of all other glycerolipids in all sampling periods at both sites. Paired depth horizons are connected by lines. Panel (E) shows results of paired t-test between T_{eff} of TGs and T_{eff} of POC. See Supplementary Table 3 for list of depth horizons shown in this figure.

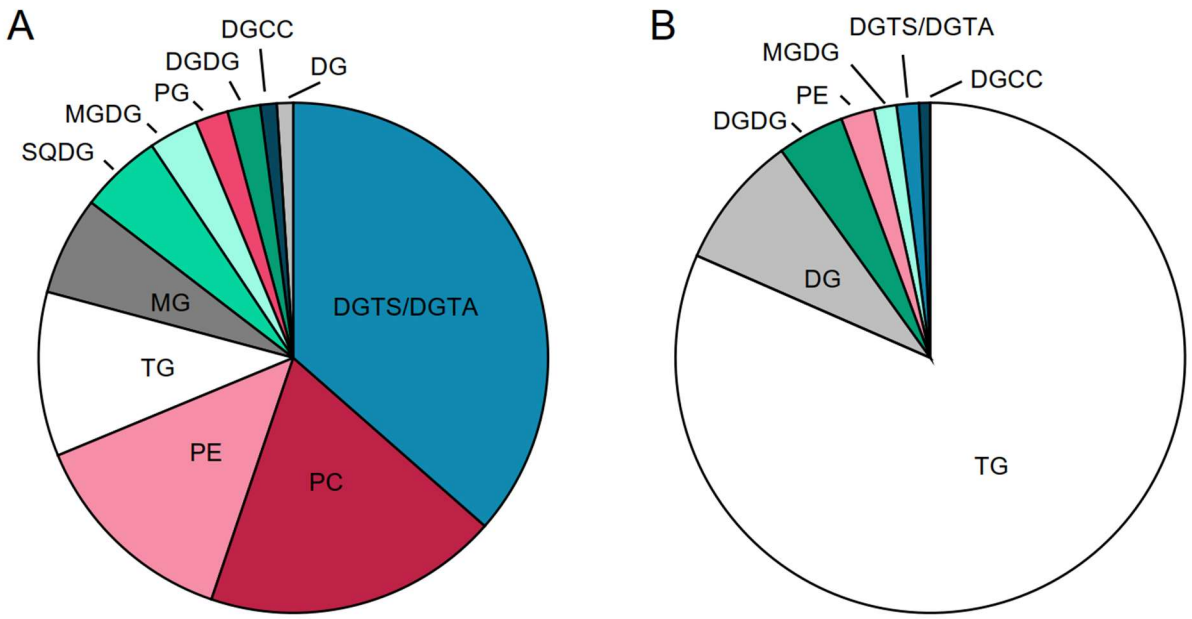

Supplementary Figure 4. Lipid species with consistently low (A) and consistently high (B) transfer efficiency (T_{eff}) across sites by class. A lipid species was determined to have a 'consistently low' T_{eff} if its transfer efficiency from the top most trap to 500 meters depth was in the bottom 50% of glycerolipids in all three sampling periods examined. Similarly, a lipid species was determined to have a 'consistently high' T_{eff} if it was in the transfer efficiency to 500 meters was in the top 50% of glycerolipids in all three sampling periods. Most lipid species did not meet either criteria; panel (A) and (B) represent 96 and 115 lipid species respectively out of 659 lipid species detectable in sinking material of both campaigns. Charts show a class proportion of the total number of lipid species in each 'consistently low' or consistently high' group, not a proportion of their flux.

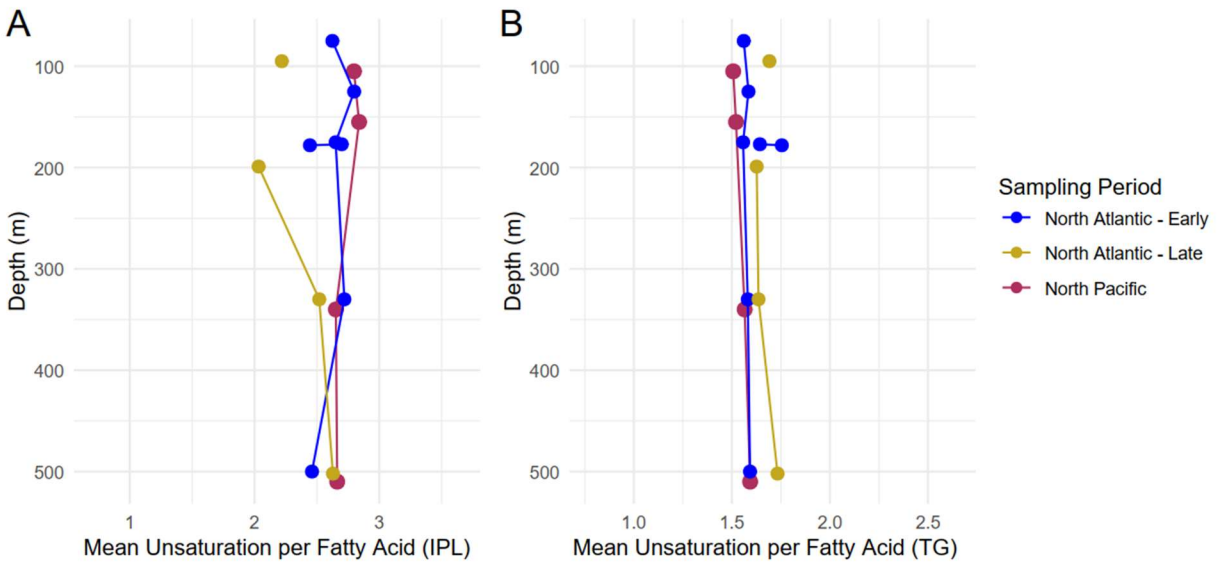

Supplementary Figure 5. Mean unsaturation per fatty for combined IPLs (A) and TGs (B) verse depth. Profiles are colored by trap sampling period. Mean unsaturation is calculated following Holm *et al.* 2022.

Holm, H.C., Fredricks, H.F., Bent, S.M., Lowenstein, D.P., Ossolinski, J.E., Becker, K.W., Johnson, W.M., Schrage, K., Mooy, B.A.S.V., 2022. Global ocean lipidomes show a universal relationship between temperature and lipid unsaturation. Science 376, 1487–1491. https://doi.org/10.1126/science.abn7455

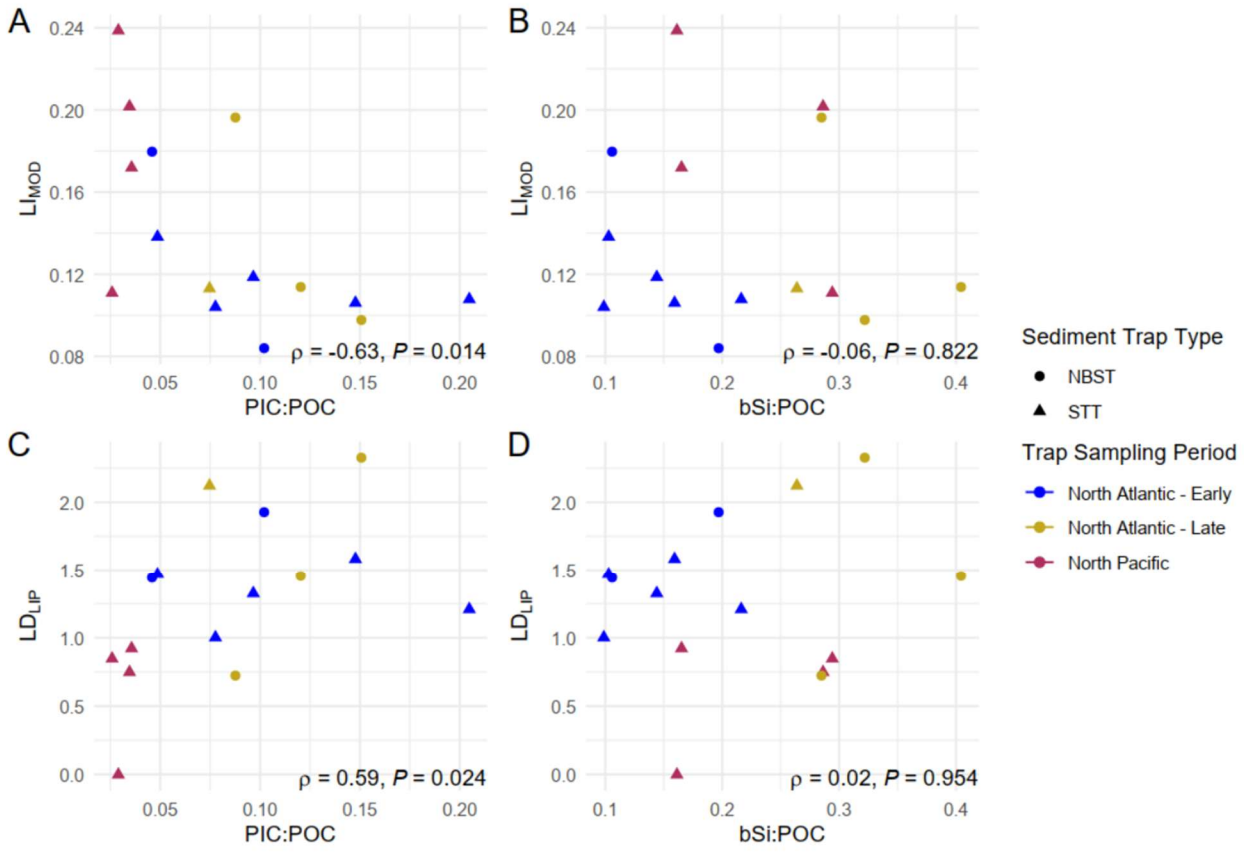

Supplementary Figure 6. Glycerolipid source and degradation indices verse bulk PIC:POC and bSi:POC ratios. Panels (A) and (B) show correlation between LI_{MOD} (lipid hydrolysis), PIC:POC and bSi:POC ratios respectively. Panels (C) and (D) show LD_{LIP} (particle type) and PIC:POC and bSi:POC ratios respectively. Spearman rank coefficient (Rho) and significance level (*p*) are shown in the bottom each panel for each relationship. The trap type (NBTS or STT) is designated with point shape. Color corresponds to the location and sampling period.

Supplementary Table 1. Lipid class abbreviations

Class Abbreviation	Full Name
DGTS and DGTA	Diacylglyceryl trimethylhomoserine and Diacylglyceryl hydroxymethyl- trimethyl-βalanine
DGCC	Diacylglyceryl-3-Ocarboxyhydroxymethylcholine
DGDG	Digalactosyl diacylglycerol
MGDG	Monogalactosyl diacylglycerol
SQDG	Sulfoquinovosyl diacylglycerol
PG	Phosphatidylglycerol
PC	Phosphatidylcholine
PE	Phosphatidylethanolamine
TG	Triacylglycerol
DG	Diacylglycerol
MG	Monoacylglycerol

Supplementary Table 2. Function coefficients, standard deviations, and means for calculating LD_{LIP}

Lipid Class	**Linear Coefficient** (β_i)	**Training Data Std. Dev.** (σ_i) [a]	**Training Data Mean** (μ_i) [a]
PE	-0.5901183	0.36882061	0.15993864
MGDG	-0.3702246	0.2085976	0.09437368
DGCC	-0.3625324	0.10524068	0.07382935
DG	-0.1007554	0.51522553	0.16102589
DGTS/DGTA	0.1318566	0.09584981	0.04031132
TG	0.2620501	0.37648114	0.1938534
PC	0.2943615	0.09192376	0.06547253
SQDG	0.5074438	0.41202908	0.17863145
PG	1.9039438	0.22876046	0.16309231

[a] Mean and standard deviation presented here are of square root transformed molar fraction data. Molar fractions for the index are calculated only using classes listed here (excluding MGs).

Supplementary Table 3. Total glycerolipid with transfer efficiencies (T_{eff}) over multiple depth horizons.

Location	Sampling Period	Type	Depth Horizon	T_{eff} of POC	T_{eff} of Total Glycerolipids [a]	Lipid Sp. w/ T_{eff}-LIP > POC [b]
			(meters)	*(% of mass)*	*(% of mass)*	*(% of Lipid Sp.)*
N. Pacific (Stn. P)	North Pacific (Epoch #3) 8/31 – 9/6 2018	STT	100 to 150	60%	92%	72%
			100 to 340	41%	33%	33%
			100 to 500	44%	18%	18%
N. Atlantic (PAP-SO)	Early north Atlantic (Epoch #1) 5/22 - 5/24 2021	STT	75 to 125	45%	46%	45%
			75 to 175	33%	53%	58%
			75 to 330	19%	29%	27%
			75 to 500	22%	25%	24%
N. Atlantic (PAP-SO)	Late north Atlantic (Epoch #3) 5/23 - 5/25 2021	NBST	200 to 330	69%	83%	75%
			200 to 500	36%	60%	55%

[a] Transfer efficiency of total glycerolipid mass combined.

[b] Percent of glycerolipid species that had an individual transfer efficiency greater than POC for said depth horizon.